OPTIMIZATION OF ELECTROMAGNETIC ACOUSTIC TRANSDUCERS FOR NONDESTRUCTIVE EVALUATION OF CONCRETE STRUCTURES

A Thesis presented to the Faculty of the Graduate school at the

University of Missouri-Columbia

In Partial Fulfillment of the Requirements for the Degree

Master of Science

By

SIVA KRISHNA CHAITANYA PENAMAKURU
Dr. Glenn A. Washer and Dr. Steven P. Neal, Thesis Supervisors

MAY 2008

The undersigned, appointed by the dean of the Graduate School, have examined the thesis entitled

OPTIMIZATION OF ELECTROMAGNETIC ACOUSTIC TRANSDUCERS FOR NONDESTRUCTIVE EVALUATION OF CONCRETE STRUCTURES

presented by Siva Krishna Chaitanya Penamakuru,

a candidate for the degree of Master of Science,

and hereby certify that, in their opinion, it is worthy of acceptance.

_____

Dr. Glenn A. Washer

_____

Dr. Steven P. Neal

_____

Dr. Roger Fales

ACKNOWLEDGEMENTS

The support and help of many people made my thesis possible. I would like to take this opportunity to thank each of them. Firstly, I would like to thank University of Missouri-Columbia and the department of Mechanical and Aerospace Engineering for giving me the opportunity for pursuing Masters Degree. I wish to express my deepest gratitude to Dr. Glenn Washer for his valuable guidance, encouragement and support throughout my research, without which it wouldn't have been possible for me to complete this work. I would like to sincerely thank Dr. Steven Neal for his immense help and valuable suggestions in completing my thesis. I would also like to extend my thanks to Dr. Roger Fales for serving as a member of my defense committee.

I am also grateful to all my friends who made this arduous Masters process an enjoyable and memorable one.

Lastly, I would like to thank my parents, brother and my grandparents for their unconditional love and support along the path of my academic pursuits.

TABLE OF CONTENTS

LIST OF FIGURES

LIST OF TABLES

ABSTRACT

There are more than 130,000 prestressed concrete bridges in the United States with about 37,000 bridges being more than 30 years old. Prestressing steel strands are an important construction element used in these bridges and are critical to their performance. Presently there is no effective Nondestructive Evaluation (NDE) technology for condition assessment of these prestressing strands once they are embedded in concrete.

The overall goal of the research is to develop an inspection technology to detect deterioration in embedded steel strands in concrete structures. The Objective of this part of the research is to optimize the design parameters of a magnetostrictive Electromagnetic Acoustic Transducer (EMAT) to maximize the sensor efficiency. EMATs are the devices used to launch and receive acoustic waves in conductive materials such as steel prestressing strands, and the propagation characteristics of these waves can be used to study deterioration, damage and tensile stresses. EMATs working on the magnetostriction principle were designed and ultrasonic measurements were made in order to maximize the efficiency of EMAT by considering the influence of modifying three parameters; bias magnetic field, number of coil turns and the number of coils. Recommendations for the design of EMATs based on this empirical study were developed.

1 INTRODUCTION

1.1 Goal/Approach

The overall goal of the research is to develop a sensor technology for the detection of deterioration in concrete structures. The sensor to be developed is an Electromagnetic Acoustic Transducer (EMAT) based on the *Magnetostriction* or *Joule* effect. An EMAT is a device that can be used to launch an ultrasonic acoustic wave (i.e. frequencies greater than 20,000 Hz) and/or detect a wave that is propagating within conductive materials such as prestressing steel bars or strands that are used to reinforce concrete structures. The sensors being developed could provide a sensing technology to support the development of smart structure technology for the long-term condition assessment and nondestructive evaluation of concrete structures. The "smart structure" concept includes designing a sensor that could be embedded within a structure and used to launch and receive acoustic waves within the embedded steel elements in concrete structures such as strands or reinforcing bars. The characteristics of these waves propagating within the embedded steel could be interpreted to detect deterioration that is occurring, such as corrosion, and could provide a method for long-term autonomous health monitoring. However a significant limitation of this approach is the low level signals of EMATs and significant attenuation that is characteristic of acoustic waves propagating in these embedded steel elements. In order to overcome this problem it is necessary to develop an optimized sensor design that increases the sensor signal-to-noise

ratio such that embedment within concrete structures is viable. A prominent step in the process of achieving the optimized sensor design is to improve the sensor efficiency by varying specific design parameters.

Hence, the objective of this study is to maximize the efficiency of a magnetostrictive EMAT by optimizing its design parameters. The magnetostrictive EMATs designed in this research primarily consisted of three elements; Core, Coil and a permanent magnet.

- Core: The core forms the basic structure of the sensor. It is made of plastic delrin material and is cylindrical in shape. The core is the part of the sensor on which windings are made.
- Coil: A copper wire was used to make windings on the core to form a solenoid type of coil. The solenoid coil (i.e. the core material along with windings made on it) is placed in such a way that it encircles the ferromagnetic material (a steel strand or a rod) under inspection. When a current is passed through the coil, it induces a time-varying magnetic field into the ferromagnetic material under inspection resulting in a change in its dimensions due to magnetostriction. The strain in the material within the aperture of the sensor results in an acoustic stress wave being propagated along the length of the material.
- Bias magnet: A rare earth magnet was used (an electromagnet could also be used) to apply the bias magnetic field. The applied bias magnetic field orders the domains of the ferromagnetic material under inspection, so that the effect of a superimposed time-varying magnetic field has the maximum effect of domain

rotations. This is an important component of using the magnetostrictive effect to launch and receive acoustic waves.

These three primary elements were used to design EMATs and experiments were conducted to evaluate the influence of modifying three parameters:

- Bias magnetic field: The variation in the amplitude of the signal generated by the EMAT for increasing bias magnetic field strengths was studied. The bias magnetic field strength was increased by increasing the number of rare earth magnets applied. The type of magnets used and the procedure followed to increase the applied bias magnetic field is described in sections 2.3 and 3.4, respectively.
- Number of coil turns: The magnetic field H, along the centerline of the coil in air, is proportional to the number of turns in coil and the current carried in the coil.

  H= ni

  Where,

  n= number of coil turns per unit length (turns/inches).

  i= electric current (amperes).

  The sensors were tested for different number of coil turns (the number of windings) and the variation in the efficiency of the sensor was reported.
- Number of coils: The effect on the amplitude of the signal generated by varying the number of coils on the core was investigated. The coils on the core were fabricated in such a way that each coil was wound in opposite direction to the adjacent coil. This counter-wound coil design provides a spatial filter that

maximizes the output signal when a wave of appropriate frequency is within the aperture of the core.

A detailed explanation about the magnetostrictive EMAT function and the basic concepts of each of these parameters is given in sections 2.2 and 2.3.

The research started with a study of magnetostriction principles. Preliminary experiments were done to develop initial design concepts launching acoustic waves into a ferromagnetic material (7-wire prestressing strand in our case). An empirical study was then conducted to identify the optimized parameters

1.2 Prestressed Concrete

This section gives a brief description of prestressing strands used in construction of concrete structures and the potential deterioration modes experienced by the strands. First, the motivation for prestressing concrete structures and various construction types are discussed.

Concrete is an amalgamated material made up of three basic ingredients; Portland cement, water and aggregates (rock, sand, gravel etc). It is a brittle material with high compressive strength (4,000 psi – 15,000 psi) and low tensile strength (100 psi – 1,000 psi). There is widespread application for concrete. It is one of the most extensively used building materials in the world. It is used as the construction material for dams, roadways, bridges, buildings, airports, power generation facilities and pipelines.

Prestressing concrete is a method of applying compressive forces to a concrete member to counteract the effects of design loads. The process of prestressing concrete helps in alleviating the tensile stresses in concrete (as concrete is low in tensile strength) and thereby control or eliminate cracking. Most concrete structures are reinforced with

steel bars to provide tensile strength. Conventionally reinforced concrete typically includes mild steel bars embedded within concrete structures that carry tensile forces. On the other hand, prestressed concrete utilizes high-strength steel bars or strands that are initially stressed in tension. The tension stresses are transferred into the concrete to provide initial compressive forces in the structure that counteract tensile stresses resulting from applied loads. Prestressing provides lighter design, improved serviceability and reduced dead load to live load ratios. Prestressing a concrete structure to alleviate tensile stresses is accomplished in the following ways:

a) Prestressed construction: In this type of construction, strands are placed in a stressing bed and stressed to a predetermined force level. Then the concrete is cast around the strands. When this concrete hardens, the strands are cut, transferring force into the concrete by a combination of chemical bonding and mechanical bonding between the strands and surrounding concrete.

b) Post tensioned construction: Concrete sections are cast with 4-6 in ducts inside the member. Strands are threaded through the ducts, anchored at either end and then tensioned. The tensile force is transferred into the section through the anchorage block. Cementitous grout or grease is then pumped into the duct to expel water and provide corrosion protection.

In both prestressed concrete structures and post tensioned concrete structures, 7-wire high strength steel strands are the common construction elements[1]. Many of the bridges in this country are constructed using prestressing tendons (strands)[1, 2].

1.2.1 Prestressing strands

A commonly used prestressing tendon material for the construction of prestressed concrete structures is a 7-wire low-relaxation prestressing strand. A 7-wire Prestressing strand is manufactured by cold drawing the high-carbon steel wire rods into wires and then stranding them. Six wires are helically wound around a straight centre wire to form a 7-wire strand. These strands have high tensile strengths ranging from 220 ksi-270 ksi[1]. These prestressing strands are arranged as individual tendons consisting of several strands or as individual strands within the concrete member.

1.2.2 Problems of Prestressing strands

Failure of prestressing strands is one factor that can contribute for the collapse of bridges and other structures. Corrosion typically plays a key role in the failure of prestressing strands. Figure 1 shows an external tendon of a post tensioned bridge that has failed due to corrosion of prestressing strands.

Figure 1: Failure of Prestressing strands in a post-tensioned tendon.

The basic types of corrosion in prestressing strands can be categorized as follows:

• Uniform corrosion

• Pitting corrosion

• Stress corrosion

In uniform corrosion, the surface of steel is uniformly affected. When the steel is left unprotected and exposed to the environment this condition can occur. Pitting corrosion occurs due to advanced uniform corrosion, resulting in the form of a localized corrosion in prestressing steel. It does not spread laterally across an exposed surface but penetrates into the metal very quickly. Two main factors contributing to pitting corrosion in concrete are presence of chloride ions and carbonation of concrete. Stress corrosion is a highly localized type of corrosion that can lead to cracking of the prestressing strand due to the high levels of tension typically present in such strands. Cracking in these cases generally originate in the base of the corrosion pit.

Depending on the prevailing corrosion type, load factors and the prestressing steel properties, the failure of prestressing strands can be classified as brittle fracture, fracture due to stress-corrosion cracking, fracture due to fatigue and corrosion[3].

- Brittle fracture:

This is caused due to exceeding load capacity. In some cases brittle fracture occurs even when the load capacity is below the fracture limit due to local corrosion attack (pitting corrosion) or hydrogen embrittlement, an embrittlement of the steel structure after hydrogen absorption.

- Fracture due to stress-corrosion cracking:

Stress-corrosion cracking is the crack formation in the prestressing strands because of tensile stresses and aqueous corrosion medium. Stress corrosion cracking can be classified as,

a) Anodic Stress corrosion:

Nitrate containing non-alkaline electrolytes (unalloyed and low alloyed) cause anodic stress corrosion cracking. Low-carbon reinforcing steels are very susceptible to this type of corrosion cracking. The prestressing strands in use today are highly resistant to this type of cracking[3].

b) Hydrogen - induced stress corrosion cracking:

Most of the fractures of prestressing strands occur due to hydrogen-induced stress corrosion[3]. The presence of hydrogen is developed from certain corrosion conditions in neutral and particularly in acid aqueous media through the cathodic partial reaction of corrosion. A sufficient load and a slight corrosion attack are required for this type of cracking.

- Fracture due to fatigue and corrosion:

Fracture due to fatigue and corrosion is the mechanical degradation of concrete structures under the joint action of corrosion and cyclic loading. When the corrosion-promoting aqueous media penetrates through a concrete crack to the dynamically stressed tendon, corrosion-fatigue cracking is possible.

1.3 Nondestructive Evaluation

This section summarizes various NDE techniques presently used for inspecting concrete bridges. First, a brief description about NDE is given.

Nondestructive evaluation is a process of evaluating the condition of a component without effecting its future use and application. The object or material under test is loaded with some form of energy and based on the response to that loading qualities of

the component are inferred. It allows the inspection of a large variety of materials and component parts. This process can be used to determine material characteristics and properties and to detect flaws and defects. Some of the uses and applications of NDE include

- To detect defects such as cracks or voids and characterize elastic properties of concrete.
- To detect defects in machine parts in aircraft industries.
- To detect defects in welds of pressure vessels.
- To detect corrosion and leakage points in pipes.
- To detect the breakage points in wire ropes.

1.3.1 Presently available inspection technologies (NDE techniques) for concrete structures

A number of NDE techniques are available for detecting flaws such as honeycombing and voids, deterioration due to corrosion of embedded steel and evaluating material properties. This section describes some of the traditionally used NDE techniques for concrete structures such as bridges.

Acoustic Emission:

The basic principle of the Acoustic Emission (AE) technique is that acoustic stress waves are emitted due to release of high energy when a flaw developed in a structure grows. By detecting these acoustic waves the deterioration in concrete structures can be monitored [4]. In this method sensors such as accelerometers are placed at or near a location where a crack is anticipated and the high energy bursts associated with crack growth are detected. The high energy wave detected is converted into electrical voltage by the sensors, and this voltage is amplified and analyzed to monitor the condition of the

structure[5]. Some other terms used to describe these phenomenon are micro-seismic emission, stress wave emission, etc.

Applications of Acoustic Emission technique (AE technique) include identifying and locating cracks and monitoring crack growth in concrete structures such as bridges[5].

Ultrasonic Pulse velocity testing:

Ultrasonic pulse velocity (UPV) testing uses Ultrasound as the input energy. Unlike in a pulse echo method (used for inspecting metals), where a single transducer is used to transmit and receive the pulse reflected from a discontinuity, a pitch catch arrangement is typically used for concrete. This arrangement is required due to high attenuation typically experienced in concrete. This attenuation results largely from scattering of the acoustic waves by the aggregates in the concrete. The pitch-catch arrangement consists of a transducer called transmitter, typically operating at 50 KHz, that is used to launch a wave into the concrete specimen under test. The wave travels through the specimen and gets scattered or reflected if there are any cracks or voids. A separate transducer placed at some distance from the first, known as receiver, is used to detect the wave. Based on the received data, this method can be used to identify subsurface voids and cracks by determining the apparent changes in the wave velocity or loss of received signal. This test procedure is conducted in accordance with the ASTM standard C597-02[6]

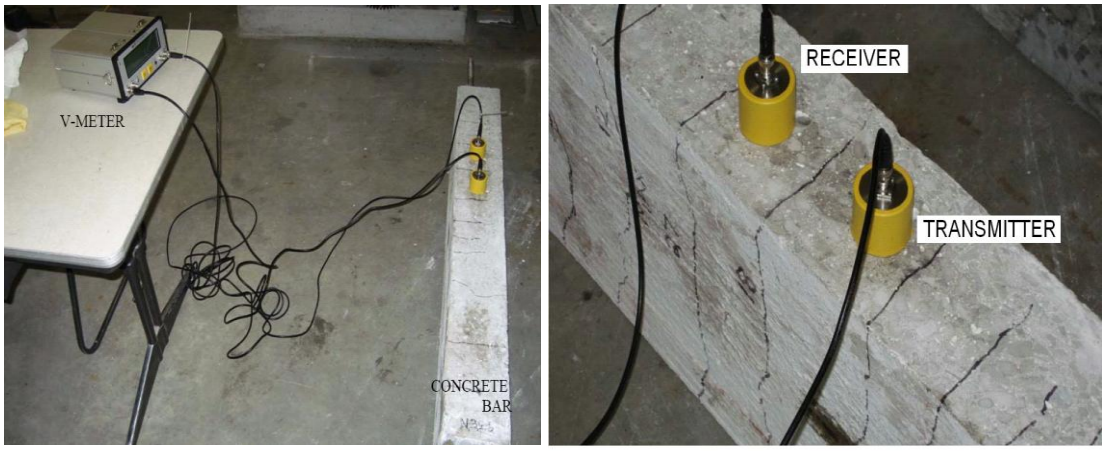

Figure 2: Photograph of a UPV system applied to a concrete beam in the laboratory.

In this technique if the velocity of the wave is known, the distance traveled by a sound wave can be determined by measuring the elapsed time or if the distance traveled is known, the velocity of the wave can be determined by measuring the elapsed time using the equation

$$V = \frac{L}{T} \tag{1}$$

Where

V= Velocity of the wave

L= Length of the path or the distance traveled by the wave

T= Time taken by the wave to travel from the first transducer (transmitter) to the second transducer (receiver)

The pulse velocity technique can also be used to assess the quality and uniformity of the concrete as the velocity of an ultrasonic pulse through a material is a function of the elastic modulus and density of the material.

$$V = \sqrt{\frac{E}{\rho}}$$

Where

V= Velocity of the wave

E= modulus of Elasticity

ρ = density of the concrete

Radiography:

Penetrating radiation from radioisotope sources, X-ray generators, and in some cases nuclear reactors, can be used to develop images of the internal features of a concrete structure (such as in the case of a medical X-ray)[7, 8]. The radiation generated by these sources is transmitted through, attenuated by, or scattered by the object under inspection. The resulting radiation can be detected using an imaging system such as film radiography, real-time radiography, or computed tomography[7]. The detected image is a two-dimensional map of the density variations in the material under test. Density variations that result from flaws in the materials appear in the image and can be interpreted by a trained inspector. Due to the ability to penetrate significant thickness of concrete this technique is used for the detection of certain internal flaws such as grout voids in post-tensioning ducts[8].

Infrared Thermography:

In this technique infrared energy emitted from the surface is used to evaluate the condition of the concrete structure. The rate of heat transfer through a material is effected by sub-surface anomalies such as delaminations. Changes in the rate of heat transfer manifests as variations in the surface temperature[8]. Using an infrared camera, an image of the surface of the material can be developed by measuring the rate at which electromagnetic energy is emitted from the material, which is highly sensitive to the

temperature of the material. The advantages of this technique are data acquisition is fast, no contact to the specimen is needed and minimum surface preparation is required[4].

Impact echo method:

Impact-echo is an NDE technique performed by applying an impact on the surface of the concrete (generally a steel ball is used to apply a transient point load) to generate waves in the concrete[9] .The waves reflected due to internal flaws and external surfaces are detected by a sensor (accelerometer or other suitable sensor) mounted on the surface. The characteristics of the detected wave, typically its frequency, are interpreted. Based on the results, the location of cracks, delaminations, honeycombing, debonding and voids in concrete structures can be evaluated. Frequency of the obtained response is given by the equation:

$$f = \frac{V}{2d} \tag{2}$$

Where,

f= frequency

V = velocity of the wave through the thickness of the concrete

d = the depth of the reflecting interface.

The disadvantage of Impact-Echo system is that it can be time consuming and labor intensive because it is a local point-by-point method. Therefore, the use on large structures is not recommended[9].

Ground penetrating radar:

In this technique, a high-frequency electromagnetic wave (frequencies between 100 MHz and 1.5 GHz or higher[10]) is launched into a concrete structure by an antenna and reflections from internal features, such as delaminated concrete, are recorded and interpreted using suitable instrumentation. This method is found useful for determining

the locations of embedded metallic materials, such as reinforcing bars or ducts in post-tensioned bridges[8]. A significant advantage to this approach is that GPR can be implemented from air-launched antennas, which allow for inspections of concrete decks to be conducted at highway speeds in some cases[8]. This technique has a potential for deep penetration at low resolutions and higher resolution at shallow penetrations. A disadvantage of the method is that results can rely heavily on expert interpretation.

In addition to above mentioned NDE techniques the most commonly used inspection technology is visual inspection for cracks by a certified inspector. This technique is low in cost and easy in application. But in this technique only the surface cracks could be inspected and the inspection surface should be able to be seen by the inspector from close range.

1.3.2 Need for new inspection technologies

Many NDE techniques are available for the inspection of concrete structures such as bridges. However, presently there is no inspection technology to detect deterioration and progressive damage such as corrosion of embedded steel elements such as prestressing strands. There are more than 130,000 bridges in US constructed using prestressing strands of which more than 37,000 bridges are at least 30 years old[11]. Most of the available NDE inspection techniques are used only for surface inspection and flaw detection of steel strands when not embedded in concrete. However, since these strands are not visually accessible once they are covered by embedded in concrete, it is important to develop a monitoring approach that evaluates the condition of the concrete structures that include these strands.

Figure 3: Collapse of a pedestrian bridge outside Lowe's Motor Speedway North Carolina.

The lack of effective inspection/NDE technologies contributed to the collapse of pedestrian bridge outside the Lowe's Motor Speedway in Concorde, North Carolina on May 2000 shown in Figure 3 and failure of Lake View drive-Interstate 70 overpass outside Washington, PA on December, 2005.

The collapse of the Silver Bridge in Point Pleasant, West Virginia, on December 15, 1967 resulting in the deaths of 46 people[12] triggered an intense interest in finding NDE methods for the detection and evaluation of fatigue cracks in steel bridges. The most recent failure of Minneapolis bridge which left 13 people dead and several injured [13]exemplify the challenges for available NDE technologies. The increase in the frequency of failure of these structures and lack of effective inspection technologies draws attention to the need for research and development of NDE technologies for condition assessment of bridges.

2 ELECTROMAGNETIC ACOUSTIC TRANSDUCERS (EMATs)

This chapter is divided into three sections. The first section gives a brief literature review regarding EMATs which includes working principles of EMATs and their advantages and applications. The second section presents the theoretical background for the operation of EMATs used in this research. The last section addresses the design of sensors used in this research.

2.1 Literature Review

A transducer that converts electromagnetic energy to acoustic energy and vice-versa is called an Electromagnetic Acoustic Transducer (EMAT). EMATs are the devices that operate on the process of electromagnetic transduction of ultrasonic waves[14]. It is the process of inducing ultrasonic waves in a solid material with the help of an electrically driven coil in the presence of magnetic field. Figure 4 shows a diagram of basic electromagnetic acoustic transducer.

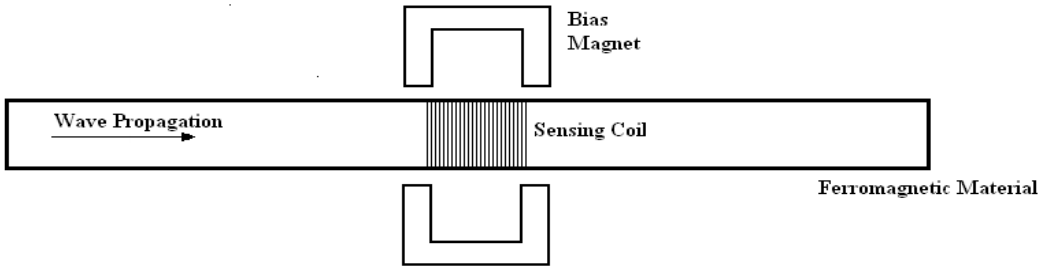

Figure 4: Schematic diagram of a Basic Electromagnetic Acoustic Transducer (EMAT).

EMATs are one of the several types of noncontact ultrasonic transducers[15, 16]. They are used for generating and receiving ultrasonic waves within the material under tests through interatomic forces, and therefore no coupling of acoustic energy is needed.

2.1.1 Working Principle of EMATs

The following section will addresses two separate types of EMATs; EMATs based upon Lorentz force mechanism and EMATs working on Magnetostriction principle.

2.1.1.1 Lorentz force mechanism:

The initial EMATs developed were for industrial use and they worked on the Lorentz force mechanism. Many designs have been proposed for the EMATs working on Lorentz force mechanism[17-19]. Considering the physics behind Lorentz force, when a coil of wire placed near the surface of an electrically conducting object is driven by an alternating current at the desired ultrasonic frequency, it produces a time varying magnetic field which in turn induces eddy currents in the material under test. If a static magnetic field is present, the interaction of these eddy currents with the static magnetic field results in a magnetic volume force whose direction and intensity is determined by the vector equation

$$F = J \times B \quad (3)$$

Where

F = Lorentz force

B= magnetic field induction

H= magnetic field

J= induced eddy current

This magnetic volume force is called the Lorentz force and this force results in the generation of a wave that propagates within the specimen. When the wave passes the region of the receiving EMAT, local eddy currents are induced in the conductive material, thus resulting in a time varying magnetic field which induces voltage in the coil by Faraday's law[18].

Disadvantages of Lorentz force EMATs:

Lorentz force EMATs have enjoyed some limited success. They are typically affected by low efficiency of transduction. Their efficiency rapidly decreases with increasing lift-off, so their use is limited to a relatively narrow gap (typically < 0.1 inch) between the sensor and the material surface[20]. As a result Lorentz forces EMATs can be difficult to implement for cable inspection and other situations where the space between the sensor and the surface may exceed one inch.

2.1.1.2 Magnetostriction Phenomenon

Magnetostriction is the changing of a material's physical dimensions in response to changing its magnetization. In other words, a magnetostrictive material will change shape (dimensions) when it is placed in a magnetic field. The change in the dimensions is the result of re-orientation of magnetic domains within the material, as domains that are

favorably aligned with the induced magnetic field grow at the expense of those less favorably aligned. As a result there is a rotation of electronic distribution at each ionic site in the lattice that causes a change in the ionic spacing. This reorientation of domains results in a strain in the material. This strain could be related to the stress by a measurable magnetostrictive constant, Γ given by the equation:

$$\Delta\varepsilon = 1/E(\Delta\sigma + \Gamma\Delta M) \quad (4)$$

Where:

$1/E = (\delta\varepsilon/\delta\sigma)_M$,

$\Gamma = (\delta\sigma/\delta M)_\varepsilon$,

E = Young's modulus of elasticity

σ = *stress*

ε = *strain*

Most ferromagnetic materials exhibit some measurable magnetostriction i.e. they experience strain when subjected to magnetic field. A detailed explanation of working of magnetostrictive EMATs designed for this research is given in section 2.2.

Advantages of Magnetostrictive EMATs:

A significant advantage of EMATs is that component under inspection need not be in contact with the EMAT. The magnetostrictive EMATs work even when there is no coupling between the sensor and the material. This helps in cable inspection and similar problems where the space between the sensor and the surface may exceed one inch. Previous EMATs designed on Lorentz force mechanism had limited ability. More traditional ultrasonic sensors which require mechanical coupling of a sensor to the

component under test face significant challenges if that coupling is to be maintained for long periods of time.

2.1.2 EMAT configurations

Depending upon the magnetic configuration and coil design different wave modes are generated and detected by an EMAT. This section describes a number of different EMAT designs and the wave modes generated by different geometric configurations.

2.1.2.1 Wave modes of an EMAT:

This section describes different wave modes for ultrasonic wave. These include Longitudinal waves, Shear waves, Rayleigh waves and Lamb waves.

a) Longitudinal Wave:

A wave in which the disturbance or vibration of the wave is parallel to the direction of propagation is called a longitudinal wave. For acoustic waves, this can be thought of as a wave consisting of alternating compressive and tensile stresses

b) Shear Wave:

A wave in which the wave disturbance is perpendicular to the direction of propagation is known as a shear or transverse wave. In the case of acoustic waves, this can be thought of as a shear stress propagating through a medium and such a transverse wave is commonly referred to as a shear wave.

c) Rayleigh Wave:

A Rayleigh wave is a type of surface wave in which the disturbance of the wave is in circular or elliptical motion to the direction of propagation

d) Lamb Wave Mode:

Similar to longitudinal waves, lamb waves have compression and rarefaction but they produce a wave guided effect due to the bounding of sheet or plate surface. Lamb waves propagation depends on the elastic material properties of a component, the test frequency and the specimen geometry. There are two primary types of lamb wave modes; Symmetric and anti symmetric.

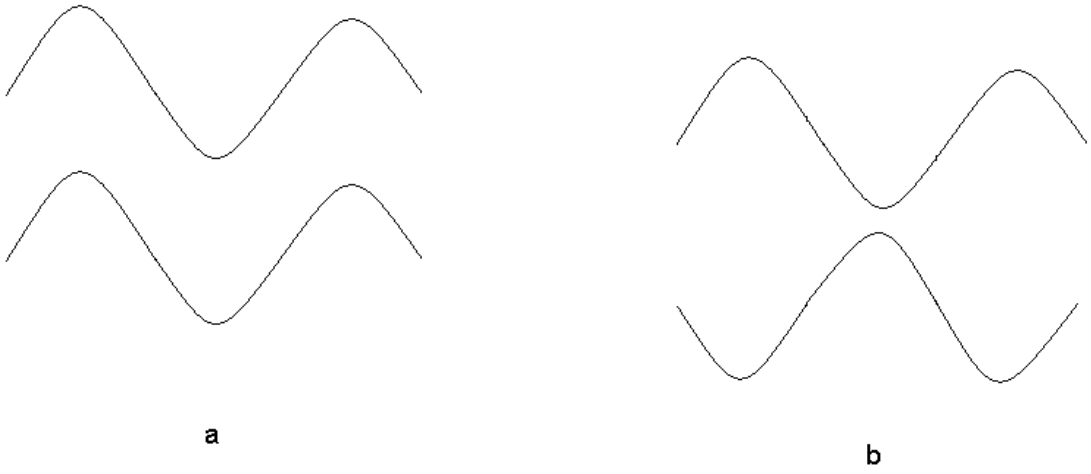

Figure 5: Diagram showing plate displacements for a) Asymmetric Lamb wave mode b) Symmetric Lamb wave mode.

Symmetrical Lamb waves move in a symmetrical fashion about the median plane of the plate. This is sometimes called the "extensional mode" because the wave is stretching and compressing the plate in the wave motion direction. The asymmetrical Lamb wave mode is often called the "flexural mode" because a large portion of the motion moves in a normal direction to the plate, and a little motion occurs in the direction parallel to the plate.

2.1.2.2 EMAT geometries

The common forms of EMAT coil configurations are: Racetrack coil, Meander coil, Spiral coil and Solenoid coil. For a given EMAT coil configuration, different types

of waves could be generated by varying the magnetic configuration and test frequency. Some of the combinations are discussed below.

Meander Coil

In this configuration there is a long coil wound back and forth along parallel lines as shown in Figure 6(a). In this configuration, by orienting the magnetic field perpendicularly to the coil, the EMAT generates rayleigh waves or vertically polarized shear waves when used on bulk solids and lamb waves when used on thin plates[21]. By placing the magnets tangentially to the coil, meander coil could be used to generate plate waves by magnetostriction. This setup can be used in steel materials.

Racetrack coil

A racetrack is a rectangular shaped long coil with rounded corners as shown in Figure 6(b). An EMAT configuration with racetrack coil and a pair of magnets placed close to the coil generates bulk shear waves that can be used for measuring speed of shear waves through a plate. When the magnets are placed tangentially to the coil, it launches compression waves[22]. In the same configuration when the magnets are aligned in the parallel direction eddy currents are generated in the same pattern of the coil. These generated eddy currents would be parallel to the magnetic field applied such that there would be no Lorentz force. Racetrack EMAT coil configuration could be used in ferromagnetic substances to generate horizontally polarized shear waves for applications such as weld flaw detection in steel plate[23]. Even a Meander coil with a similar magnetic set up could be used for the same application.

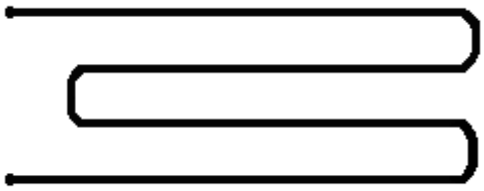

a)

b)

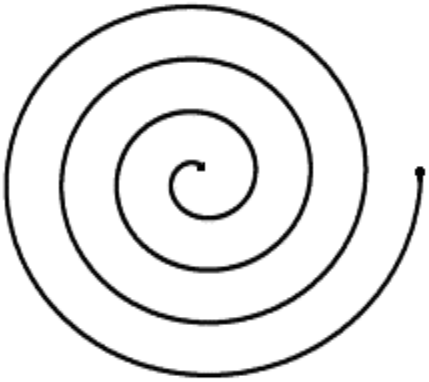

c)

Figure 6: Picture showing the EMAT coil configuration of a) Meander coil b) Racetrack coil c) Spiral coil.

Spiral Coil

In this configuration, the coil is wounded in concentric circular from as shown in Figure 6(c). This coil is also called as Pancake coil. This configuration is primarily used to generate bulk shear waves. A spiral coil could also be used to generate longitudinal waves by magnetostriction when the static magnetic field is oriented parallel to the coil. This type of coil configuration has been used to inspect large areas of steel plate structures

Solenoid coil

Here a coil is wound around the specimen under inspection or around a core material of some diameter as shown in Figure 7. The coil encircles the specimen under inspection.

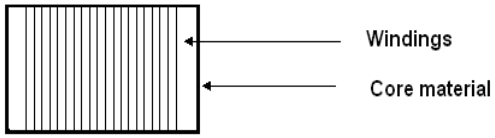

Figure 7: Solenoid coil.

This configuration is used to launch and receive longitudinal waves employing Joule effect. Using appropriate bias field configuration, the ability of solenoid coil to detect flexural waves (anti-symmetrical lamb wave)has been reported[24].

2.1.3 Advantages and applications of an EMAT

Some of the advantages of EMAT are:

- EMATs do not need coupling which allows easy automation, high speed scanning, high temperature inspection and reduces the potentially detrimental effects of coupling variations on measurements.

- Minimal wear on component under test and no surface preparation is needed.
- It provides all the advantages of Ultrasonic testing plus some unique capabilities make it the technique of choice for :

a) Defect detection (surfaces, weld seams, volumes) in automated environments

b) Non destructive evaluation of materials at high temperatures.

The applications of EMAT include:

a) Flaw detection in steel bars: An EMAT system has been designed for flaw detection (seams and laps) of steel bars[19]. This design used a pulsed magnet and generated Rayleigh waves.

b) EMATs are used for flaw detection in welds. For examining the aluminum welds in the external liquid fuel tanks of a Space shuttle, NASA is using a portable EMAT system [25].

c) As EMATs don't require a fluid couplant, they have been used for ultrasonic applications at high temperature.

d) EMATs have been successfully used for applications ranging from flaw detection to thickness gaging and stress measurement in strands [8,26] .

2.2 Theoretical Background

This section gives the theoretical foundation for the working of magnetostrictive EMATs designed for this research

Magnetostriction is the process in which the change in the dimensions of the material takes place due to the result of re-orientation of magnetic domains within the material in the presence of magnetic field. The EMATs designed for this research work on the *Joule* effect often called as longitudinal magnetostriction.

Joule magnetostriction:

When a coil of wire is wound on a ferromagnetic rod or on a core material encircling the rod and an alternating current is passed through the wire, a time varying magnetic field is produced by the coil which couples to the ferromagnetic rod. The magnetic field H, along the centerline of the coil in air is proportional to the number of turns in coil and the current carried in the coil.

$$H=ni \tag{5}$$

Where,

n= number of coil turns per unit length(turns/in)

i= current(amps)

This magnetic field coupled to the rod causes it to change its length (in the dimension parallel to the applied field) due to Magnetostriction. Assuming the applied frequency is high, in the ultrasonic range, this strain is localized near the coil due to inertia of the rod. This localized strain propagates as an acoustic stress wave, at a speed of sound, in both the directions along the length of the rod. This coil acts as a transmitter.

A second coil is wound on the core material encircling the rod and it acts as a receiver. When the propagating acoustic pulse reaches this receiver coil in the receiver, it causes a change in the magnetic induction of the material via the inverse-magnetostrictive effect. This change in the magnetic induction of the material induces an electric voltage in the receiving coil by the Faraday Effect

$$V = -NA\frac{dB}{dt} \tag{6}$$

Where,

N= number of turns

A= cross-sectional area

$\frac{dB}{dt}$ *= time rate of change of magnetic induction field*

The induced voltage change in the receiving coil is subsequently amplified, conditioned, and processed using appropriate test setup.

Wave equations for Joule effect:

An element of volume of mass P dxdydz is considered at some point "y" inside the core of the transmitting coil. Due to a current "i" flowing in the coil windings, a magnetic field H exists inside the core of the transmitting coil.

The equation of motion for this elemental volume is given by

$$\rho \frac{\partial^2 u}{\partial t^2} = \frac{\partial T}{\partial y} \tag{7}$$

Where,

u = displacement,

ρ= density

T = Total stress acting on the volume element

The basic magnetostrictive equations that relate stresses to strain are given by[27]

$$H = \frac{1}{u_r} B - 4\Pi\lambda \frac{\partial u}{\partial y} \tag{8}$$

$$T = E_a * \frac{\partial u}{\partial y} - \lambda B \qquad (9)$$

Where,

λ = *magnetostrictive constant,*

E_a = *Young's modulus at constant flux,*

B = *flux density,*

$\partial u / \partial y$ = *strain*

u_r = *relative permeability*

Equations (7), (8) and (9) form the basis for the longitudinal stress wave propagation for the system under consideration. For a given coil geometry and a given current, H can be determined. Equations 7, 8 and 9 could be solved to get the quantity of interest i.e. displacement "u", since it yields in the form of strain and also generates the flux in the output coil.

Substituting B from (9) into (8) ;

$$T = E_a * 1 - \left[\frac{4\Pi\mu_r\lambda^2}{E_a} * \frac{\partial u}{\partial y}\right] - u_r\lambda H \qquad (10)$$

Let

$$E = E_a * \left[1 - \frac{4\Pi\mu_r\lambda^2}{E_a}\right]$$

Where,

E= *Young's modulus at constant field intensity*

The constant $\frac{4\Pi\mu_r\lambda^2}{E_a}$ is usually small hence E becomes approximately equal to E_a.

Substituting E in equation (10) gives

$$T = E \frac{\partial u}{\partial y} - u_r \lambda H \qquad (11)$$

Substituting equation (11) into equation (6) gives,

$$\frac{\partial^2 u}{\partial y^2} - \frac{1}{c^2}\frac{\partial^2 u}{\partial t^2} = \frac{u_r \lambda}{E} * \frac{\partial H}{\partial y} \qquad (12)$$

Where $c = \sqrt{(E/\rho)}$, is the velocity of the longitudinal sound wave in the medium

Equation 12 is the standard wave equation with an inhomogeneous term that contains the driving magnetic field whose distribution in space and time is known.

Bias magnetic field:

The bias magnetic field is used in an EMAT to maximize the magnetostrictive effect. The bias field orders the domains along the axis of the rod prior to the application of a time varying magnetic field. Once the time varying magnetic field is applied, the domains that are initially oriented along the axis of the rod undergo maximum reorientation when the superimposing field varies over 360 degrees.

Using these basic electromagnetic concepts and knowledge from previous research, EMAT transducers were designed to launch and receive acoustic waves in ferromagnetic rods.

2.3 Design of EMATs

This section describes the design of EMATs which were made as a part of this study. EMATs were made with a core of delrin material, magnets used to apply bias magnetic field and windings used to apply time-varying magnetic field.

2.3.1 Core Design

The Core is the part of the sensor on which windings are made. The Core of the EMAT was constructed of machined plastic delrin material with periodic coil spacing. Cores of 1, 2, 4 and 8 periodic coil spacing were made. These cores were made in order to test the performance of the sensor for different number of coils. Since the velocity of acoustic wave in a material is normally fixed, at a given frequency, transducers launch and receive waves by having appropriate distance between the windings selected to match the equation 3[28].

$$f = \frac{V}{2D} \qquad \textbf{(3)}$$

Where D= Distance between the coils.

The distance between the windings provides a spatial filter that will preferentially detect and generate waves at the desired frequency. The dimensions of the EMAT core made are as shown in the Figure 8.

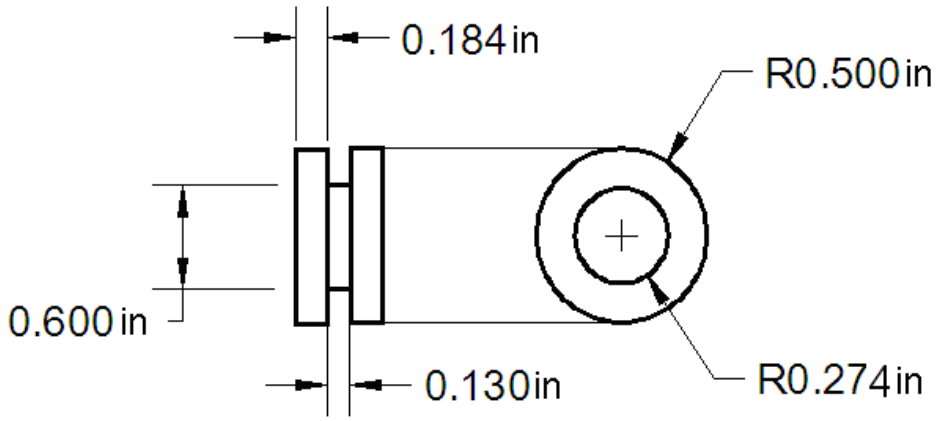

(a)

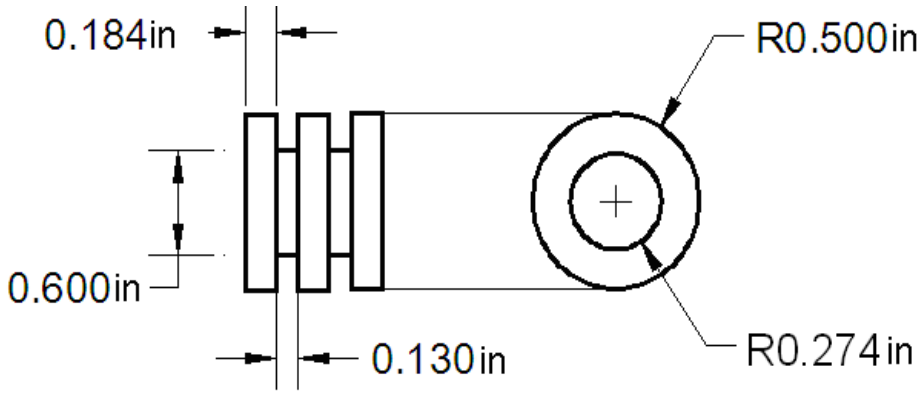
0.184in
R0.500in
0.600in
0.130in
R0.274in

(b)

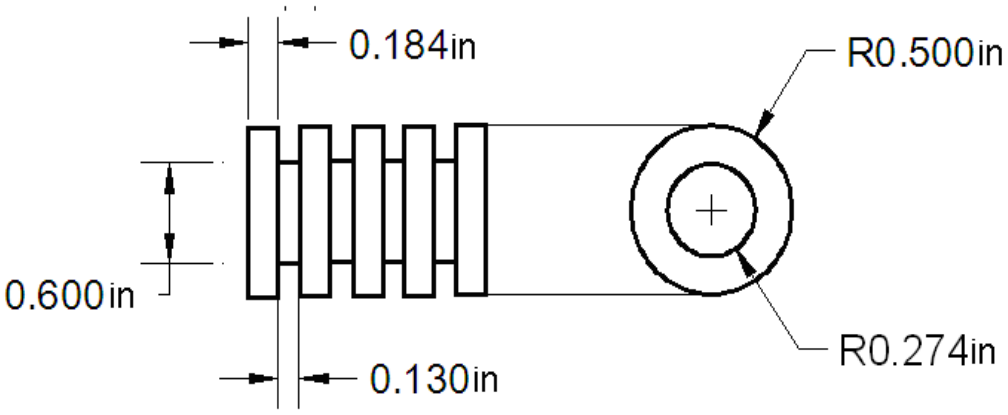
0.184in
R0.500in
0.600in
0.130in
R0.274in

(c)

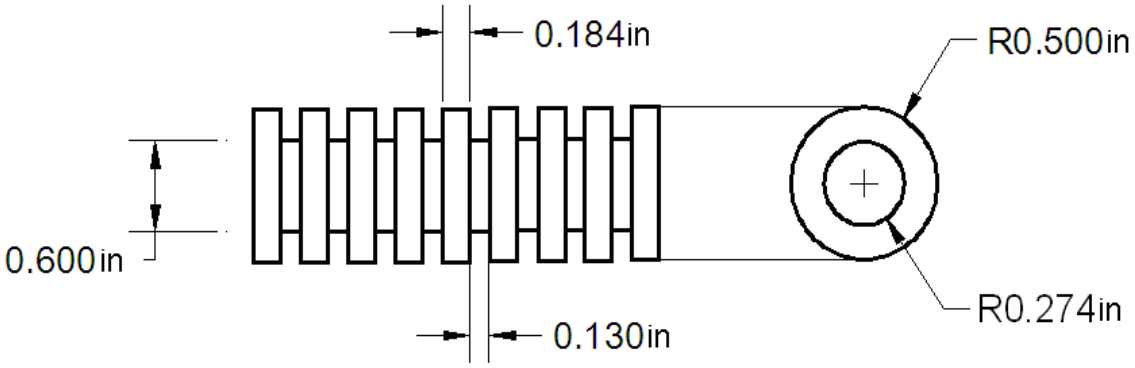

(d)

Figure 8: Diagram of the sensors with dimensions a) 1-coil sensor b) 2-coil sensor c) 4-coil sensor d) 8-coil sensor.

The core of the EMAT was placed on a 7-wire Prestressing strand (such that it encircles the strand). The diameter of the Prestressing strand used in our experiment was approximately 0.5 inches and the inner diameter of the cores used was 0.548 inches.

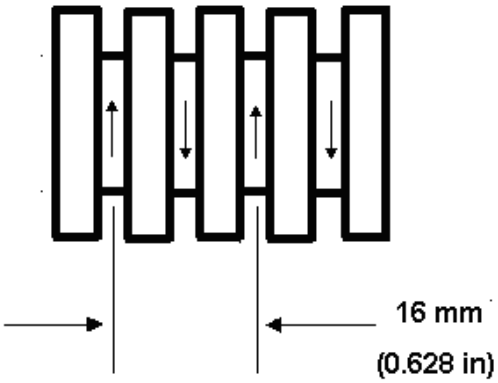

Figure 9: Periodicity of an EMAT. Arrows on core indicate the direction of windings.

The width of each coil is approximately 0.13 inches. At a nominal frequency of 0.32 MHz, the period of the coils is equal to the wavelength of the waves generated in the strands i.e. approximately 16 mm or 0.628 inches as shown in Figure 9.

2.3.2 Coil Windings

A copper wire was used to make windings on the coils of the EMAT core. Initially 50 windings were made on each coil. Figure 10 shows the 1, 2, 4 and 8-coil sensors with windings on them.

Figure 10: Pictures showing the 1-coil, 2-coil, 4-coil and 8-coil sensors with windings.

The windings were made in opposite direction on each coil as shown in the Figure 9. The arrows on the core shown in Figure 9 indicate the direction of winding. The counter-wound coil design provides a spatial filter that maximizes the voltage output when the wave of appropriate frequency is within the aperture of the sensor i.e. when the strain wave generated from the transmitter passes through the periodically spaced coils of the receiver, it sonically resonates the incoming strain wave.

2.5.2.3 Magnets

Rare earth permanent magnets were used to apply the bias magnetic field of the EMAT. The magnets used were cylindrical Neodymium Iron Boron (NdFeB) magnets,

grade 30 Neodymium disc magnets(1inch diameter, 0.1 inch thickness) and grade 35 Neodymium disc magnets(0.875 inch diameter,0.375 inch thickness) with nickel coating . The magnetic field strength along the centre of the magnets was measured to be around 600 Gauss for cylindrical magnets, 1200 Gauss for grade 30 Neodymium disc magnets and around 3500 Gauss for grade 35 Neodymium disc magnets. The magnetic field was measured using a gauss meter.

The cylindrical magnets were used by placing them at the ends of the EMAT core to provide the bias magnetic field while the disc magnets were used by placing them in a magnetic circuit setup as shown in Figure 11.

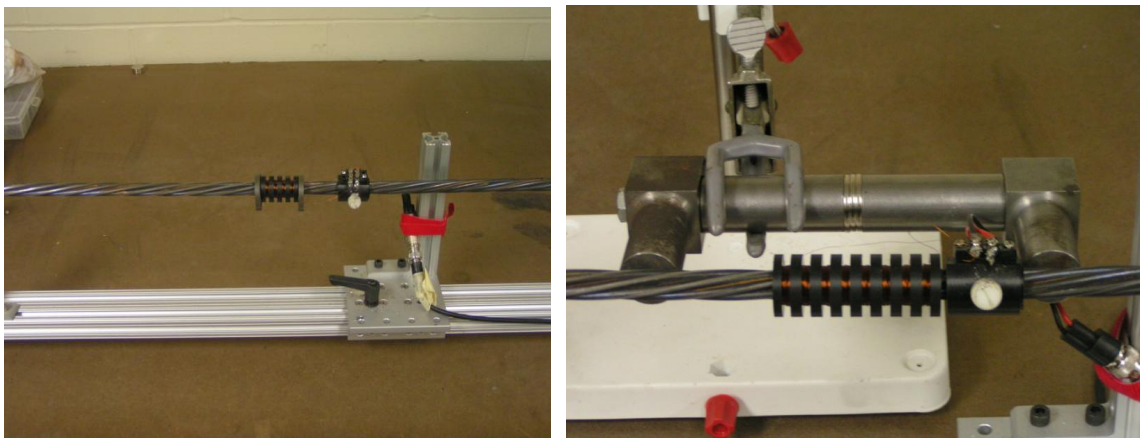

Figure 11: Photographs showing the EMAT cores with Cylindrical magnets at the ends of the core (left) and magnetic circuit design(right).

The type of magnets used for each sensor depended upon the test setup and the experiments done as discussed in section 3.4.

3 EXPERIMENTAL

The experiment design consisted of EMATs used to transmit and receive ultrasonic waves and appropriate test setup to record the amplitude of the waveforms detected by the EMATs. Preliminary testing conducted to establish basic sensor performance is described in section 3.1. Section 3.2 describes the basic experimental setup used for the research and section 3.3 explains the physics of pulse propagation in a prestressing strand. The next three sections (3.4, 3.5 and 3.6) discuss the tests conducted as a part of this study and various setups used for that purpose and section 3.7 summarizes the same. The last section (3.8) discusses the measurements made as a part of this study.

3.1 Preliminary testing

A preliminary test was conducted to develop initial design concepts and gain an understanding of sensors performance characteristics. In these tests, coils of wire were formed by winding directly on the prestressing strand. Windings were made at 4 different locations on the surface of the strand. Each winding was wound in the opposite direction to the adjacent winding. An arbitrary spacing of approximately 2 inches was used for this initial testing.

Figure 12: Prestressing strand with windings.

Both the ends of the windings were soldered to a connector which is in turn connected to the oscilloscope through an amplifier. The end of the strand was impacted with a hammer to launch a mechanical pulse in the strand that could be detected by the coil sensor. The sample waveform shown in Figure 13 is the pulse detected by the windings displayed in the Oscilloscope.

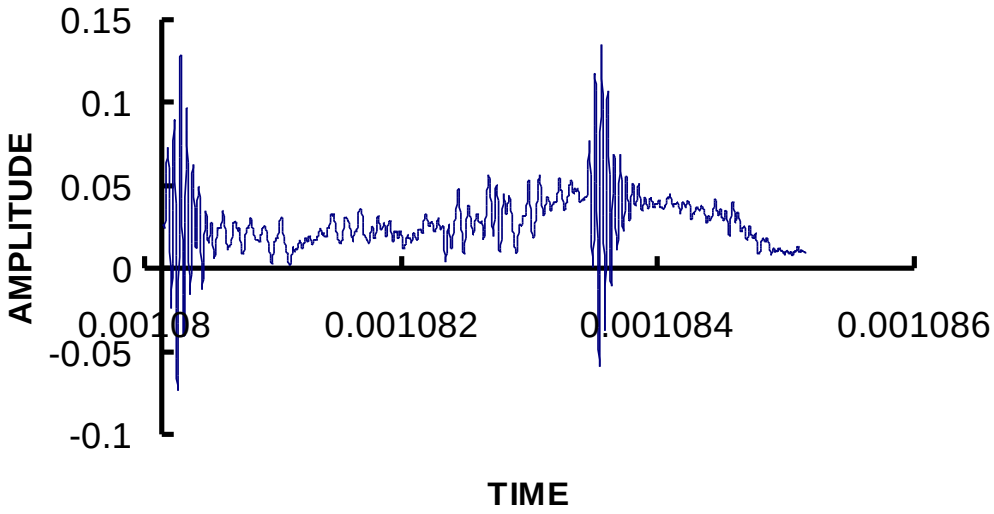

Figure 13: Picture showing the amplitude of the signal generated when a prestressing strand (having 4 windings of 50 turns each) was hit by an iron material.

The strand was initially tested by making windings at 4 places on the prestressing strand with 30 turns made on each winding. The test was repeated by increasing the number of turns on each winding to 50 and further tests were conducted by increasing the number of turns on each winding to 70 turns. Waveforms were detected for 50 turns per winding and 70 turns per winding while no waveform was detected for 30 turns per winding. The initial number of windings to test the sensors was decided to be 50 turns per winding. This initial testing illustrated the basic operation of the coil based sensor developed in this research.

3.2 Experimental Setup

The basic experimental set up is shown in the Figure 14. A 7-wire Prestressing strand was supported by plastic connectors mounted on an aluminum rail. The strand was unstressed, and a slight curvature of the strand due to spooling can be seen in Figure 14.

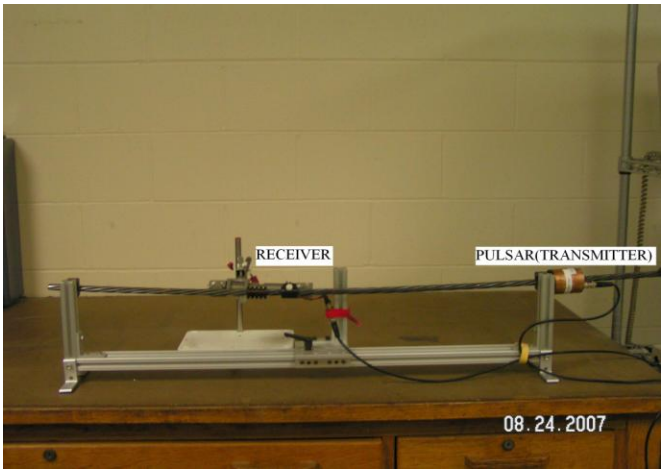

Figure 14: Prestressing strand with the transmitting and receiving sensors.

Two sensors separated by a distance of approximately 22 inches were placed on the strand. One sensor acted as a transmitter to launch acoustic waves in the strand. The sensor acting as pulser (transmitter) in the set up is the 3-coil sensor. The second sensor

acted as a receiver to detect acoustic waves. The description of the sensor, acting as receiver in the setup shown in Figure 14 is given in section 2.3.

3-coil sensor: A 3-coil sensor (acting as the transmitter in Figure 13) was used as a standard sensor to provide consistent pulser or receiver properties to evaluate the variations in transducer properties i.e. for the experimental tests conducted in this study, the test setup consisted of two sensors. One sensor was the 3-coil sensor used to provide consistent pulser or receiver properties (depending upon the test conducted) while the other sensor was used to evaluate the changes in the efficiency by varying its design parameters as explained in the objective of this study.

The 3-coil sensor had 70 windings per coil and windings were made in opposite direction on each coil. The bias magnetic field for this sensor was provided by cylindrical magnets. Copper shielding tape is used to wrap the 3-coil sensor in order to reduce the ambient electromagnetic interference[11]. The design parameters of the 3–coil sensor remained constant in all the experiments conducted in this study. In the remainder of the thesis the 3-coil sensor would be referred as the “Standard Sensor”.

The schematic diagram for the experimental setup is given in Figure 15.

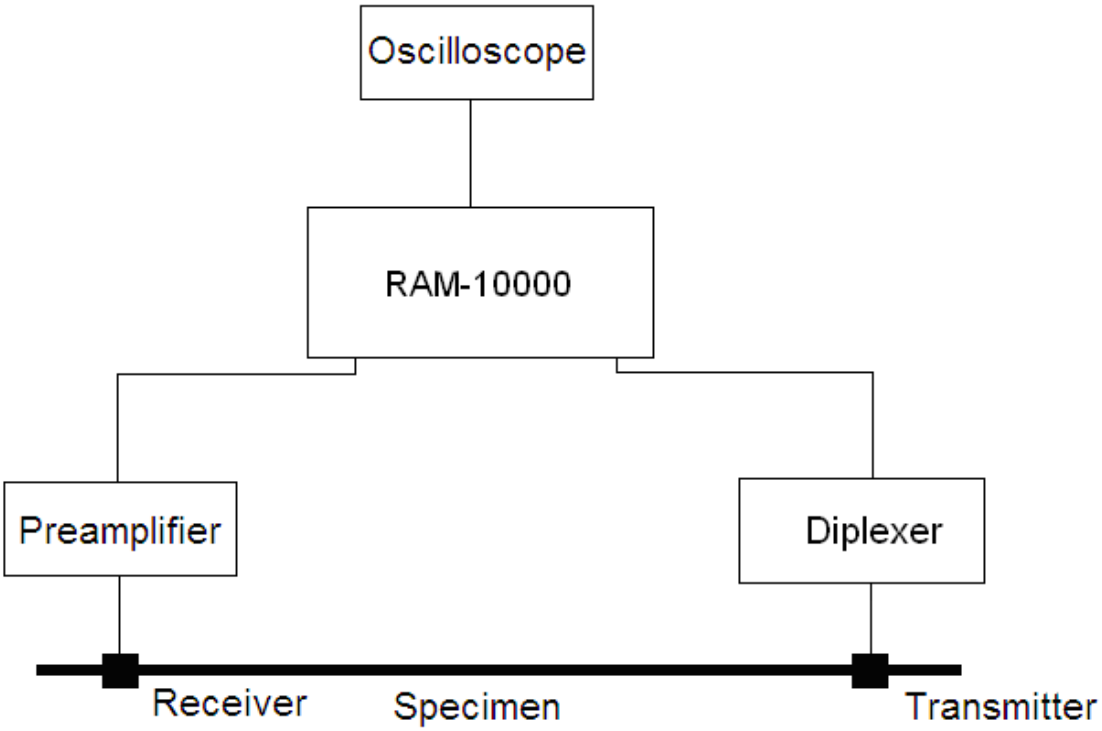

Figure 15: Schematic diagram of the experimental setup.

The transmitter is connected to Ritec RAM-10000 through a diplexer. The RITEC RAM-10000 is an ultrasonic measurement system used for the ultrasonic research and applications of the nondestructive evaluation of materials properties. The instrument is able to provide short (down to single cycle) burst excitations to power transducers. The instrument utilizes a fast switching, synthesized continuous wave (CW) frequency source to produce the transmitting signal. In our test setup, the RAM 10000 was used to provide a high current pulse to the transmitter and to control input parameters such as frequency and receiver gain.

The receiver sensor is connected to preamplifier which in turn is connected to the RAM-10000 receiver circuits and subsequently fed to a high-speed digital oscilloscope. The 40 dB preamplifier connected to the receiver is used to amplify the low level signals detected by the receiving transducer. The amplified received signals are sampled and averaged 64 times and displayed on a HP Infinium 54815A digital oscilloscope. The sampling rate used was 10 Msa/s. Figure 16 shows the experimental set up consisting of prestressing strand with two sensors connected to the ultrasonic equipment.

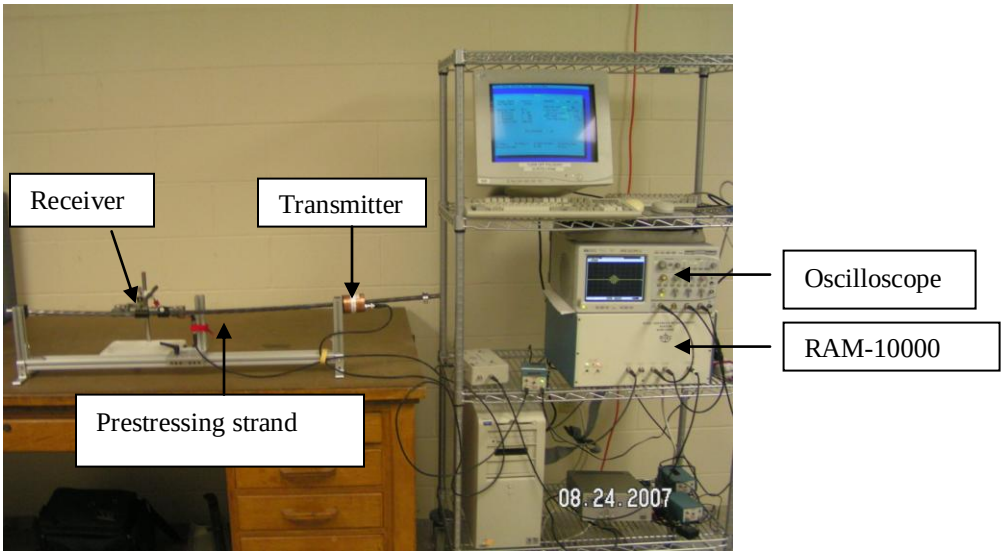

Figure 16: Photograph showing the experimental setup including the prestressing strand, EMAT transducers and RAM 10000 instrument.

3.3 Pulse propagation in strands

When an electrical pulse is applied to the transmitter (pulser) coil, the portion of the strand below the coil changes its dimension due to magnetostriction resulting in a longitudinal stress wave being transmitted along the length of the rod. This wave propagates in both the directions, and when this wave reaches the receiver coil, it causes a change in the magnetic induction of the material due to inverse-magnetostrictive effect. The resulting voltage change induced in the receiver coil is amplified and recorded by the

oscilloscope. Figure 17 shows a schematic diagram of the pulse propagation in a strand sample.

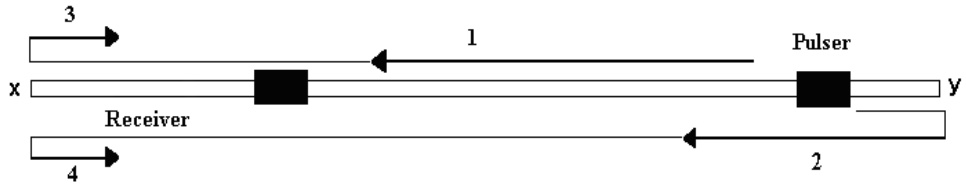

Figure 17: Pulse transmission in a prestressing strand.

From the above Figure 17 it can be seen that "x" and "y" are the receiver end and the transmitter end of the rod respectively. As explained earlier, when a current pulse is induced into the transmitter, a wave is generated in the rod due to magnetostriction. This wave propagates along the rod in both the directions as 1(traveling towards receiver end "x") and 2(traveling towards end "y") as shown in the Figure 17. Wave 1 reaches the receiver and due to inverse-magnetostrictive effect it causes a voltage change in the receiver that is recorded in the oscilloscope (shown as pulse "1" in Figure 18).Wave 2 reaches the end "y", gets reflected back and reaches the receiver generating a voltage change (shown as pulse "2" in Figure 18). Whenever a wave reaches the end of the rod and gets reflected back there is a loss of energy resulting in some attenuation of the wave amplitude. Wave 1 further travels along the rod, reaches the end "x", gets reflected (shown as wave 3 in Figure 17) and reaches the receiver generating a pulse (shown in the Figure 18 as pulse 3). The wave 2 travels from the receiver, gets reflected at end "x" (shown as wave 4 in Figure 17) and reaches back at the receiver generating a pulse "4". This process of the pulse traveling along the rod getting reflected back at the ends continues until the amplitude of the signal gradually diminishes to zero due to damping.

These pulses 1, 2, 3, 4… are recorded in the oscilloscope which is connected to the receiver sensor through an amplifier.

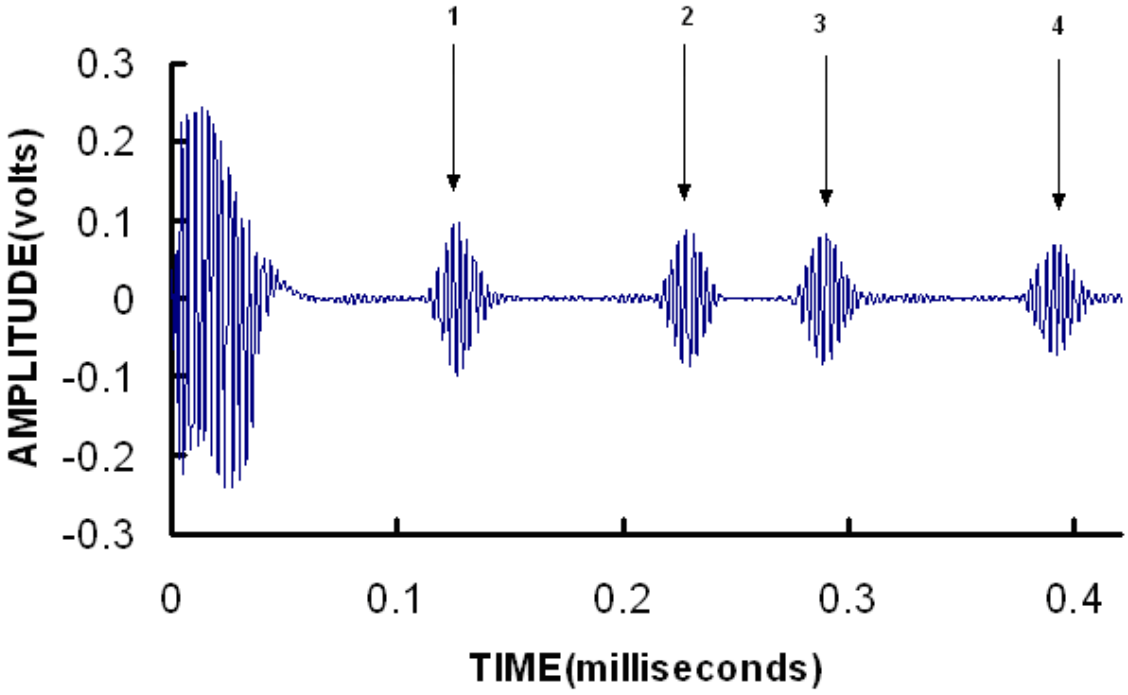

Figure 18: Pulses detected by the 4-coil magnetostrictive EMAT.

From Figure 18 it can be seen that amplitude of pulse "1" is slightly greater than pulse "2" (= pulse "3") which in turn is slightly greater than pulse "4". This is because pulse "1" has been produced by wave 1 that reaches the receiver directly while pulse 2 and 3 are produced by waves 2 and 3 that reach the receiver after getting reflected at the ends y and x respectively resulting in some attenuation and pulse 4 is caused by wave 4 that reaches the receiver after getting reflected at the ends twice.

Performance of single pulse is taken into consideration for these experiments conducted in order to maximize the amplitude of the signal generated. The pulse considered is the pulse traveling directly from the transmitter to the receiver without end

reflection i.e. pulse “1” and in the remainder of the thesis this pulse would be referred as “main pulse” or “main signal”.

3.4 Magnetic field tests

Experimental tests were conducted to investigate the effect of bias magnetic field levels on sensor efficiency. Two different setups were used. The initial set up consisted of magnets placed at the ends of the sensor while the second set up had the magnets placed in a magnetic circuit. Detailed discussion of the magnetic setups used, magnetic field measurements made and the magnetic field experiments conducted is provided in the following sections.

3.4.1 Test set up for cylindrical magnets

The initial magnetic field test arrangement utilized cylindrical rare earth magnets placed at both ends of the sensor core. The experimental set up for this testing is as shown in the Figure 19.

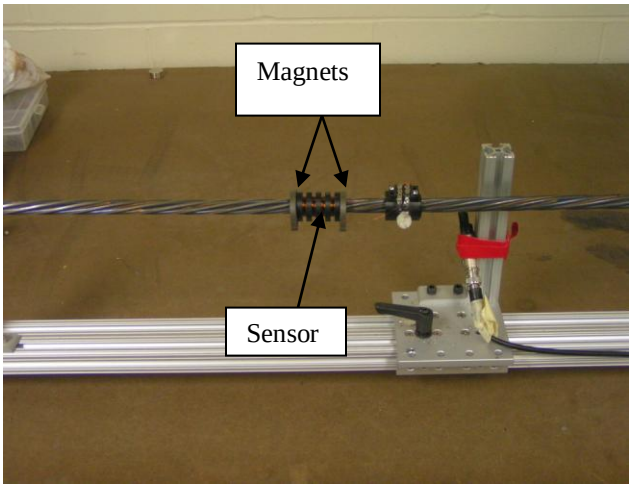

Figure 19: A 4-coil sensor with magnets placed at both ends of the sensor.

The sensors were tested for increasing magnetic fields by increasing the number of cylindrical magnets at either ends of the sensor. Initially the testing was conducted by placing 1 magnet each at either end of the sensor. Later the sensors were tested by adding 1 more magnet at the either end (making a total of 2 magnets at each end) and further tests were conducted by adding 1 more magnet at either ends (making a total of 3 magnets at each end) and this procedure was repeated till there were 7 magnets each at either ends of the sensor. In each case, the amplitude of the main signal or main pulse detected by the sensor was recorded in the oscilloscope.

Magnetic field measurement

Magnetic field measurements were made in air by placing the cylindrical magnets at the ends of the sensors. Initially 1 magnet was placed at each end of the 2-coil sensor. The magnets and the sensor were aligned in such a way that their center-axis remained the same. The probe of the gauss meter was moved along the center-axis of the sensor (with 1 magnet each at its ends) and the maximum magnetic field values were recorded using the gauss meter.

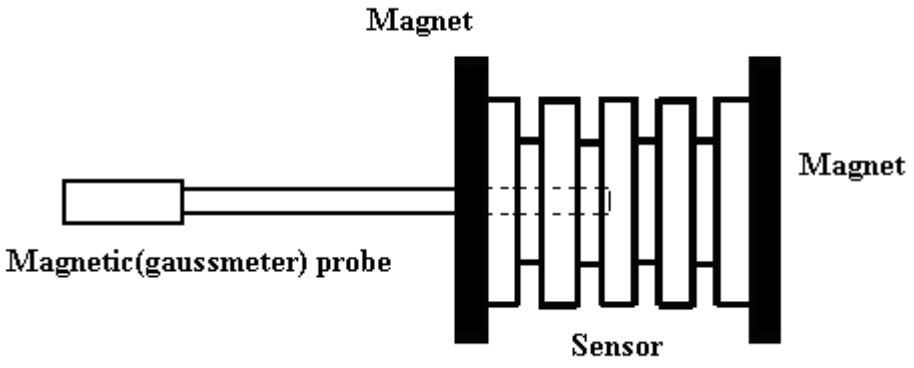

Figure 20: Magnetic field measurement of a 4-coil sensor.

Later 1 more magnet was added at both the ends of the sensor making 4 magnets in total (2 on each side) and the maximum magnetic field values were recorded. The tests

continued until there were 7 magnets on each side of the sensor. The tests were repeated for all the sensors and respective magnetic field measurements were recorded. The maximum magnetic field was observed when the probe was half way through the sensor. Figure 21 shows the magnetic field values recorded for different sensors.

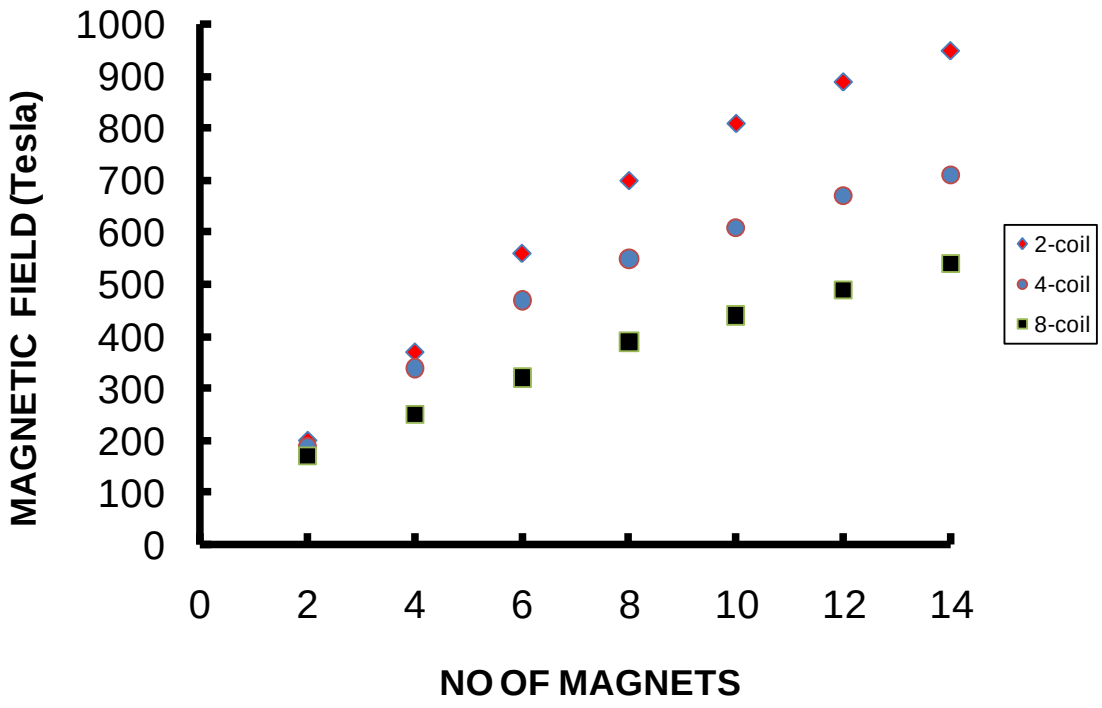

Figure 21: Graph showing the maximum magnetic field values recorded with an increase in the number of magnets for a 2-coil, 4-coil and an 8-coil sensor.

From the above graph it could be noted that the magnetic field values recorded for the 2-coil sensor was greater than the 4-coil sensor which is in turn greater than the 8-coil sensor. The reason for this could be explained as follows. In the present setup, as the magnetic field is provided by the magnets placed at the ends of the sensors, the effect of magnetic field on the sensor weakens as the distance between the magnets increases. In this case, as the magnets are placed at the ends of the sensor, the distance between the

magnets increases with an increase in the length of the sensor. As a result, as the length of the sensor increased (2-coil < 4-coil < 8-coil) the magnetic field values recorded decreased (2-coil> 4-coil > 8-coil).

3.4.2 Magnetic circuit setup

In this setup the magnets were placed in parallel to the sensor as shown in Figure 22. These magnets were held by two low carbon steel pole pieces that couples the magnetic field to the strand.

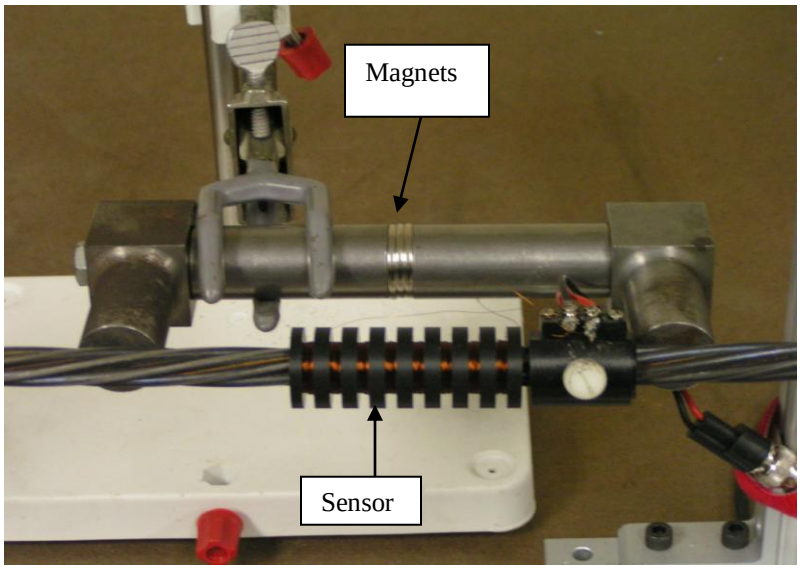

Figure 22: Magnetic setup.

The magnets used in this testing were grade-30 Neodymium disc magnets (1 inch diameter, 0.1 inch thickness) and grade-35 Neodymium disc magnets (0.875 inch diameter, 0.375 inch thickness) with nickel coating. A combination of both these type of magnets was used to test the sensors for an increasing magnetic field. The magnetic field was increased by increasing the number of magnets placed in between the poles. Initially the sensors were tested by placing a single disc magnet (grade-30 Neodymium) between the poles. Later 1 more grade-30 Neodymium magnet was added making it a total of 2

magnets and the sensors were tested for 2 magnets. Later 1 more was added and the tests continued till there were 8 Neodymium disc magnets (grade-30) between the poles. A combination of grade-30 Neodymium disc magnets and grade-35 Neodymium disc magnets was used to further increase the magnetic field. Sensors were tested by placing a combination of 8 Neodymium disc magnets (grade-30) and 2 Neodymium magnets (grade-35) between the poles. Later 2 more neodymium magnets (grades 35) were added and the sensors were tested for 8 Neodymium disc magnets (grade-30) and 4 Neodymium magnets (grade-35) placed between the poles. The corresponding waveforms of different amplitudes generated by the sensors were recorded in the oscilloscope.

Magnetic field measurement

In this setup the applied magnetic field was measured at the end of both the poles using a gauss meter and the corresponding values were recorded. In this case the number of coils of the sensor does not effect the magnetic field value. The magnetic field value measured changes only with change in the number of magnets. The minimum magnetic field value obtained with these magnets was 180 gauss when a single grade-30 Neodymium disc magnet was used while the maximum field obtained was around 325 gauss when a combination of 8 Neodymium disc magnets (grade-30) and 4 Neodymium magnets (grade-35) were used.

In order to obtain a magnetic field value of less than 180 gauss, cylindrical magnets were used in the place of disc magnets in the magnetic circuit set up. The lowest magnetic field measured was of 80 gauss when a single cylindrical magnet was used.In spite of using magnets of higher strength in this case, the magnetic field values obtained for these experiments were in the range of 80 gauss-325 gauss, which is smaller than the magnetic field values obtained in the previous setup where only cylindrical magnets were

used. This is because in the previous set up magnetic field measurements were made in air by placing the cylindrical magnets at the end of the sensor, while in the present setup the measurements were made at the end of the poles while the magnet is held between the poles. This is a qualitative measure of the magnetic effect. There was no common method of measuring the magnetic field for these two configurations.

3.4.3 Magnetic field test matrix

Sensors as receivers

The goal of this test is to study the effect of increasing bias magnetic fields of the receiver on the amplitude of the main signal detected by the receiver. In these tests, the standard sensor(refer section 3.2) was placed as the transmitter in all the cases while one of the sensors designed for this research (e.g. 1-coil) was placed as the receiver. The bias magnetic field level of the receiver was increased and the corresponding waveform detected by the receiver was recorded. Later the test was repeated with the other sensors (2-coil, 4-coil and an 8-coil) while they were placed as receivers. Two different setups were used to provide the bias magnetic field for the receivers. The first setup used the test setup for cylindrical magnets while the second setup used the magnetic circuit setup. The tests were repeated in both the setups and in both the setups the sensors (1-coil, 2-coil, 4-coil and 8-coil) were tested for increasing magnetic fields. The number of windings per coil was 50 for all the sensors.

Sensors as transmitters

The goal of this test is to study the effect of increasing bias magnetic fields of the transmitter on the amplitude of the main signal detected by the receiver. The experimental setup had the standard sensor used as a receiver in all the cases while one of the sensors designed for this research (e.g. 1-coil) was used as the transmitter. The bias

magnetic field level of the transmitter was increased and the corresponding waveform detected by the receiver was recorded. Later the test was repeated even with the other sensors (2-coil, 4-coil and an 8-coil) while they were placed as transmitters. The magnetic circuit setup was used to apply the bias magnetic fields for these sensors (transmitters). The number of windings per coil was 50 for all the sensors.

3.5 Testing for Number of coils

This section deals with the tests conducted to study the effect of number of coils on the performance of the sensor. It could be understood from the previous section that in the magnetic field tests itself the tests for number of coils was included as the sensors of different number of coils (1-coil, 2-coil, 4-coil and 8-coil) were tested for varying magnetic fields. However in order to study only the influence of number of coils on the efficiency of the sensor and to have a better analysis the other parameters are considered to be kept constant. For this purpose two sets of tests (receiver and transmitter tests) were further conducted by varying the number of coils when the other parameters like magnetic field and number of coils turns are kept constant. They are discussed as follows.

Sensors as receivers

The aim of this test is to investigate the effect of change in the number of coils of the receiver on the main pulse detected by the receiver. The experimental set up had the standard sensor placed as the transmitter in all the cases while the number of coils (1-coil, 2-coil, 4-coil and 8coil) in the receiver was varied. In each case the amplitude of the signal detected was recorded. The magnetic field applied was constant for all the receiver sensors and at 240 gauss. This constant applied magnetic field was selected arbitrarily and was obtained by using single neodymium 35-grade disc magnet in the magnetic

circuit setup. The number of windings per coil was constant and at 50 turns for all the sensors.

Sensors as transmitters

The aim of this test is to study the effect of change in the number of coils of the transmitter on the main pulse detected by the receiver .The experimental set up had the 3-coil sensor with 70 windings placed as the receiver in all the cases while the number of coils (1-coil, 2-coil, 4-coil and 8coil) in the transmitter was varied. In each case (1-coil, 2-coil, 4-coil and 8coil) the amplitude of the main signal detected by the receiver was recorded. The magnetic field applied was constant and a single 35-grade neodymium magnet was used in the magnetic circuit setup (refer 3.4.2) to apply the bias magnetic field. The applied magnetic field was 240 gauss, selected arbitrarily. The number of windings per coil was constant and was 50 turns for all the sensors.

3.6 Testing for different number of coil turns

Sensors were tested for different number of coil turns with the bias magnetic field applied being the same in all the cases. The magnetic circuit setup was used to apply the bias magnetic field. The sensors (1-coil, 2-coil, 4-coil and 8-coil) were placed as receivers and were tested for increasing number of coil turns. The change in the amplitude of the signal with the change in the number of coil turns of the receiver has been recorded. Based on the results the number of coil turns could be optimized for each sensor.

3.7 Summary of the test matrix

The information represented in the following table summarizes the tests conducted as a part of the study

Test conducted		Bias magnetic field and test setup	Number of coils	Number of turns per coil
Magnetic field tests	Receiver	Two setups used. Cylindrical and magnetic circuit setup. Tested for varying magnetic fields.	1-coil, 2-coil, 4-coil and 8-coil	50 turns per coil for each sensor
	Transmitter	Tested for varying magnetic fields. Magnetic circuit setup was used	1-coil,2-coil,4-coil and 8-coil	50 turns per coil for each sensor
Number of coils tests	Receiver	Tested at constant magnetic field. Magnetic circuit setup was used	1-coil,2-coil,4-coil and 8-coil	50 turns per coil for each sensor
	Transmitter	Tested at constant magnetic field. Magnetic circuit setup was used	1-coil,2-coil,4-coil and 8-coil	50 turns per coil for each sensor
Number of windings tests (Receiver tests)		Tested at constant magnetic field. Magnetic circuit setup was used.	1-coil,2-coil,4-coil and 8-coil	1-coil—50, 75, 100, 150, 250 turns per coil 2-coil—50, 75, 100, 150 turns per coil 4-coil—50, 75, 100, 150 turns per coil 8-coil—40, 50, 75 turns per coil

. **Table 1: Table showing tests conducted as a part of the study.**

* Receiver tests: In all the receiver tests, sensors of different number of coils were placed as receivers while the standard sensor was placed as a transmitter. The variation in the main pulse detected by the receiver by varying the design parameters (magnetic field, number of coils, no of coil turns) of the receiver is recorded and analyzed.

** Transmitter tests: In all the transmitter tests, sensors of different number of coils were placed as transmitters while the standard sensor was placed as a receiver. The variation in the main pulse detected by the receiver by varying the design parameters (magnetic field, number of coils, no of coil turns) of the transmitter is recorded and analyzed.

3.8 Power and peak amplitude measurements

Experiments were done to optimize the design parameters of the EMAT. The results were analyzed based on two factors, the peak amplitude and the average power of the main pulse generated by the sensors. The peak amplitude gives the value of the highest peak of the signal generated by the sensor and the average power value signifies the magnitude of the main pulse per unit time detected by the sensor.

a) The peak amplitude: It is the absolute value of the highest peak in a pulse generated by the sensor.

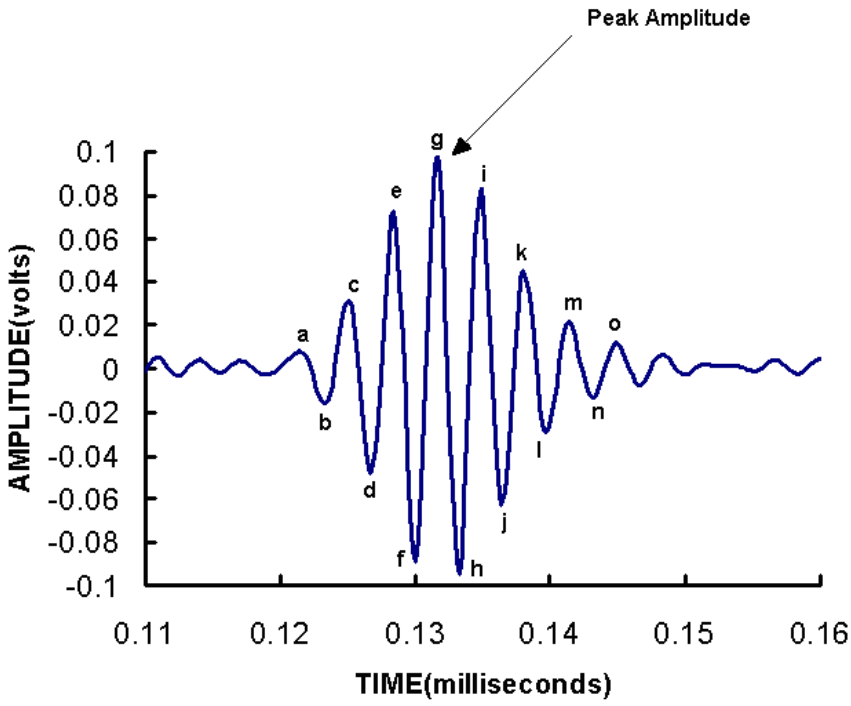

Figure 23: Graph denoting the amplitude peaks of a pulse.

From the Figure the amplitude peaks in the pulse are denoted by a, b, c, d…..m, n, o. The highest amplitude peak is denoted by "g".

b) Average power of the pulse:

Power of the pulse signifies the magnitude of a signal per unit time and it is the area under the curve shown in Figure 24.

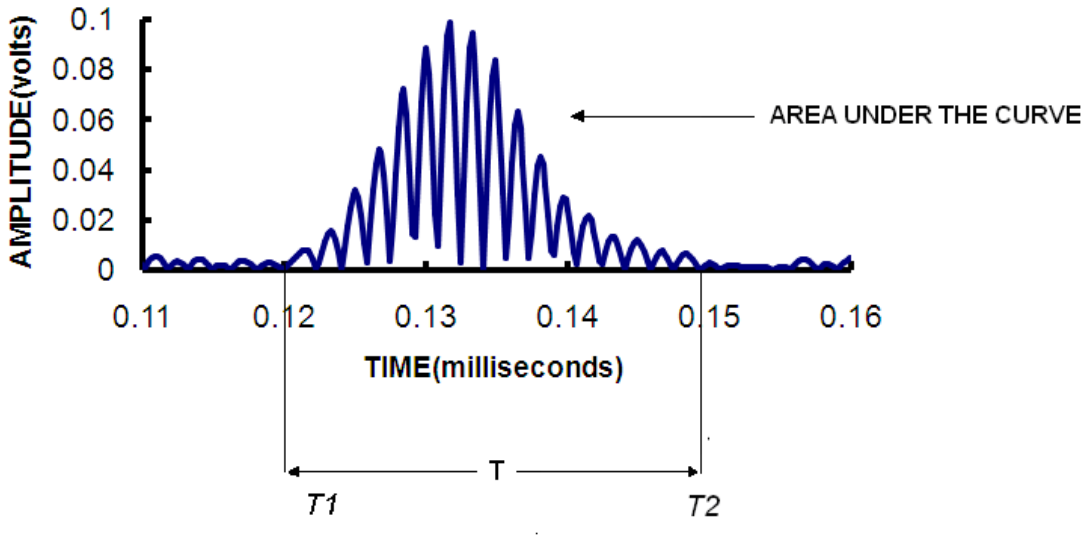

Figure 24: Graph showing the area of the pulse under the curve.

The Curve shown in Figure 24 is drawn using the absolute values of the amplitude peaks (a, b, c, d….o) of the signal shown in Figure 23. Power of the pulse is given by [29]

$$P = 1/T \int_{T_1}^{T_2} s(t)^2 \, dt \qquad (2)$$

Where,

s(t) is the value of the signal at a given time 't".

s(t) is the value of signal amplitude (voltage) in our case.

$T = T_2 - T_1$.

"T" is the time period of a pulse. It differs according to the number of cycles in a pulse.

4 RESULTS/DISCUSSION

4.1 Magnetic Field Tests

The sensors were tested for different magnetic fields with the number of windings per coil being constant for all the sensors. The amplitudes of the main signal detected by the sensors were recorded and the graphs were drawn for various magnetic fields. As the trends produced by all the sensors (1-coil, 2-coil, 4-coil and 8-coil) were almost similar, to reduce the abundance of data, the results produced by only 2-coil, 4-coil and 8-coil are represented in this section. The results produced by 1-coil are not represented as it had the least impact on the efficiency of the sensor.

4.1.1 Magnetic field tests results when the sensors of different number of coils were placed as receivers

The following section describes the results obtained for the magnetic field tests done by placing the sensors of different number of coils (1-coil, 2-coil, 4-coil and 8-coil) as receivers and the standard sensor (refer section 3.2) as a transmitter. The tests were done by increasing the bias magnetic field levels of the receiver and respective amplitudes of the signals detected for different magnetic fields were recorded. The first set of tests was done using cylindrical magnets placed at the end of the sensors. The second set of tests used the magnetic circuit setup described in section 3.4.2. In both the cases the sensors were tested for increasing magnetic field and the tests were repeated for all the coils.

4.1.1.1 Magnetic tests using cylindrical magnets

This section represents the test results obtained using the setup for cylindrical magnets. The input voltage for the test was 0.8 V and the receiver gain was 30 dB. Figure 25 and 26 show the power and the peak amplitude of the pulse detected by the sensors for different magnetic fields.

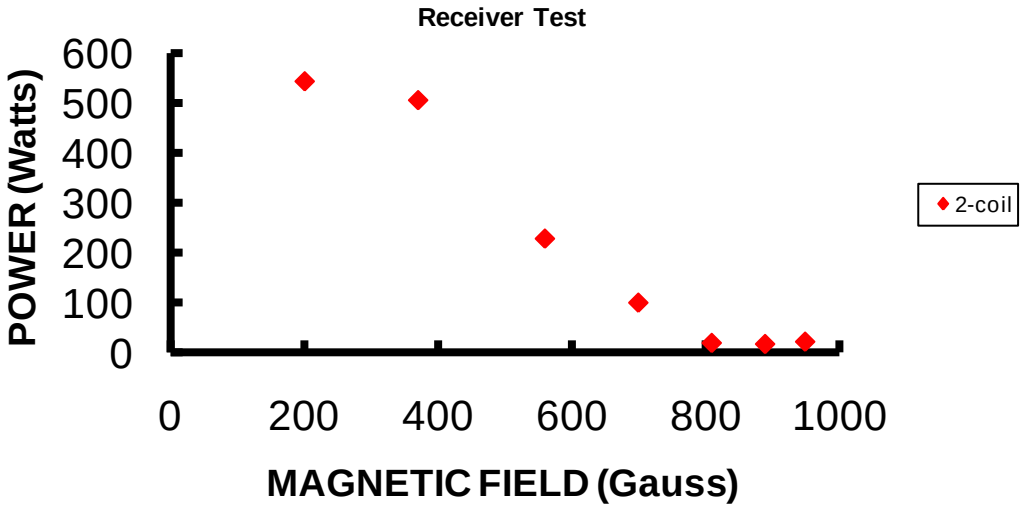

a)

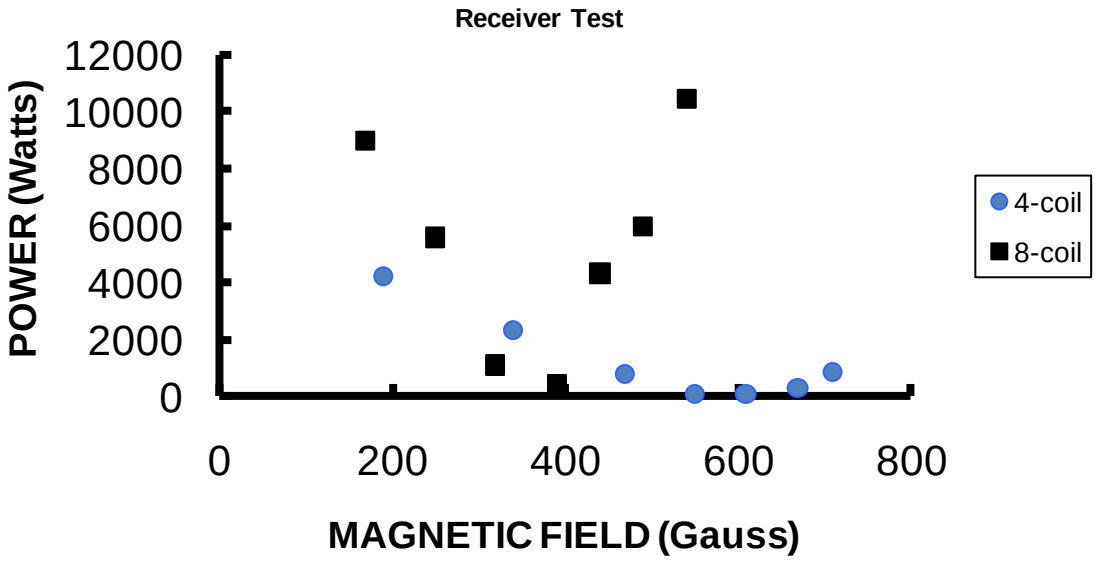

b)

Figure 25: Graph showing the trend between the Magnetic field and power of the pulse detected by a) 2-coil sensor b) 4-coil and 8-coil sensor.

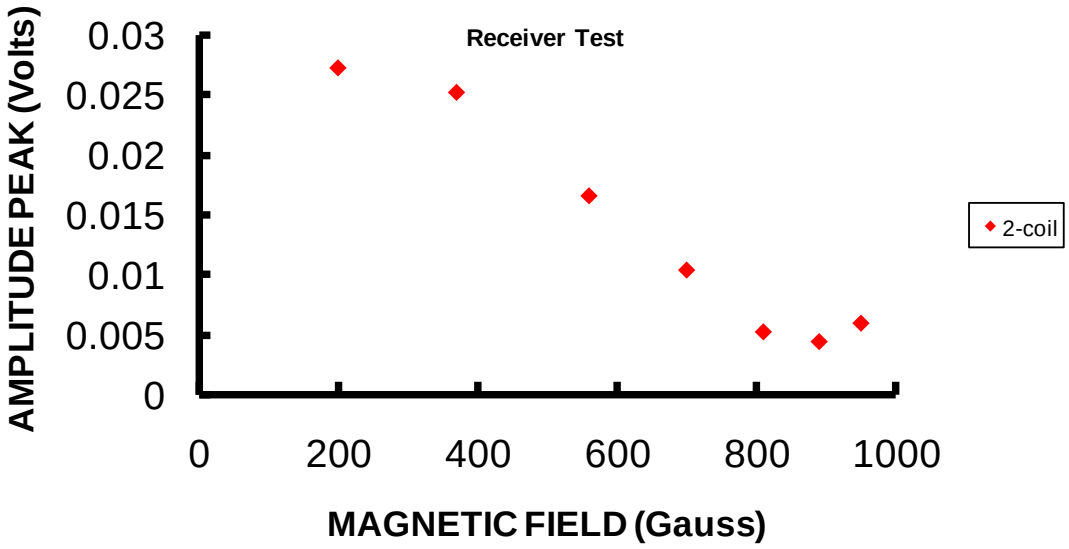

a)

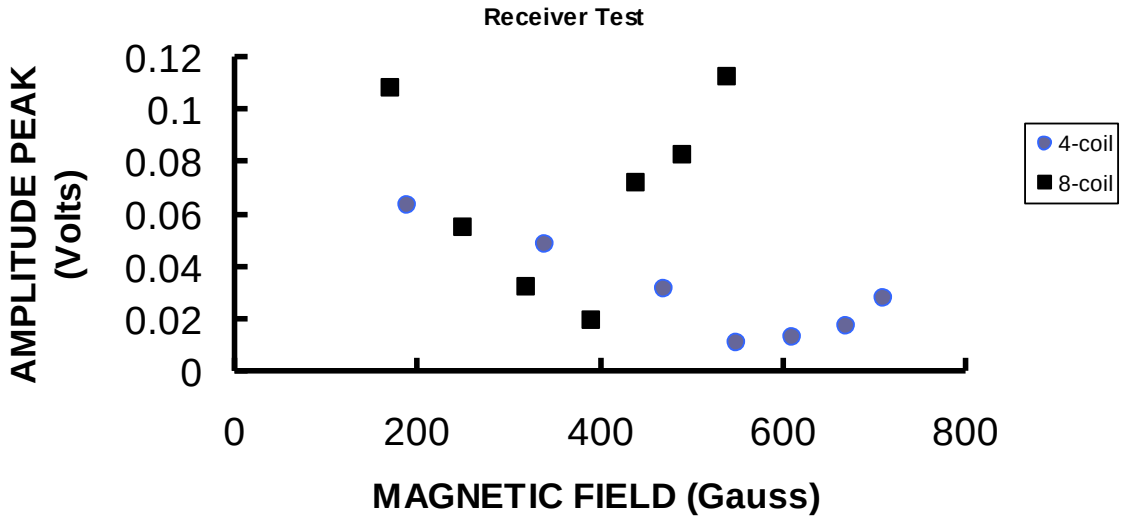

b)

Figure 26: Graph showing the trend between the Magnetic field and the peak Amplitude of the pulse detected by the a) 2-coil sensor b) 4-coil and an 8-coil sensor.

Initially there was a decrease in the amplitude of the signal with an increase in the magnetic field and with a further increase in the magnetic field the amplitude started increasing. From both the graphs (Figure 25 and Figure 26) it could be observed that there was an increasing trend in the amplitude of the signal after an initial decrease for all the sensors.

4.1.1.2 Results for testing of sensors using magnetic circuit setup

This section represents the test results obtained using the magnetic circuit setup. The voltage of the input signal for all the sensors was 0.6 V and the receiver gain was 22 dB. The following table gives the information on the number of windings and the magnetic field applied to each sensor.

Sensor	Number of Coil turns	Magnetic field
2-coil	100(50 per coil)	80-325 gauss
4-coil	200(50per coil)	80-325 gauss
8-coil	400(50 per coil)	80-325 gauss

Table 2: Table showing the type of sensor, number of coil turns made on the sensor and the minimum and the maximum values of the magnetic fields applied.

The minimum field applied was 80 G and the maximum magnetic field applied was 325 G. The tests were repeated for all the sensors. 50 windings per coil were made on all the sensors. Figure 27 and 28 show the power and the peak amplitude of the pulse detected by the sensors for different magnetic fields.

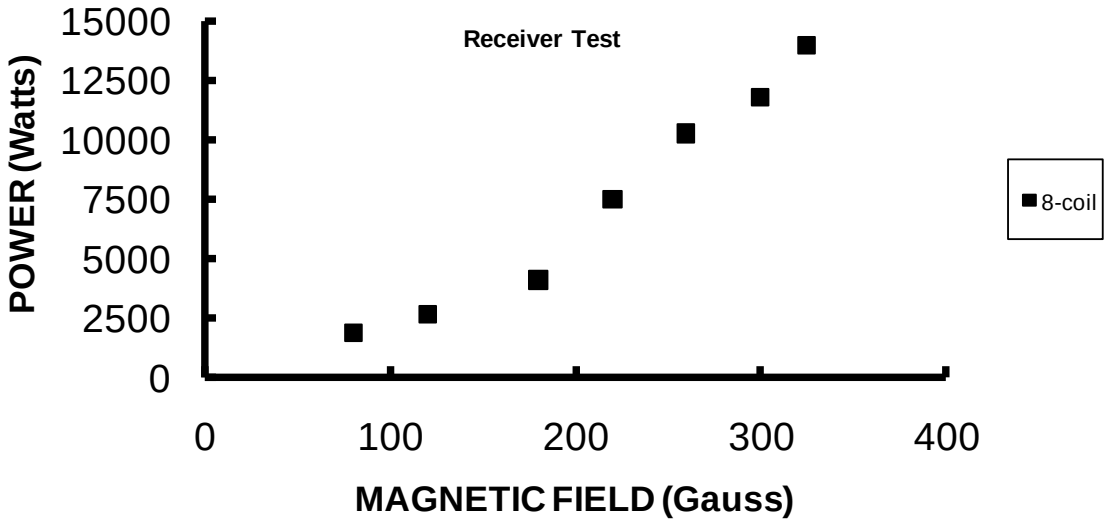

a)

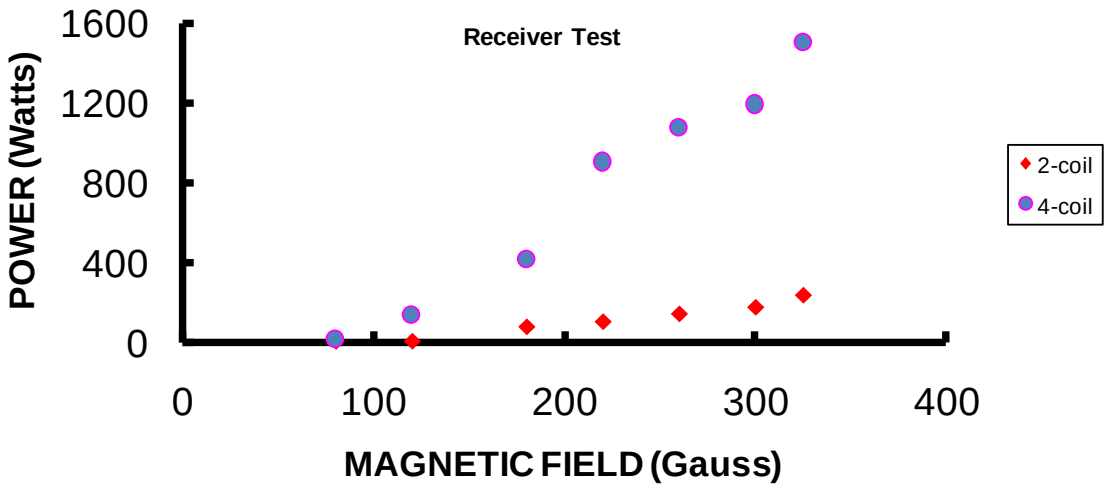

b)

Figure 27: Trend between the power of the main pulse detected and the magnetic field applied for a) 8-coil sensor b) 2-coil and 4-coil sensors.

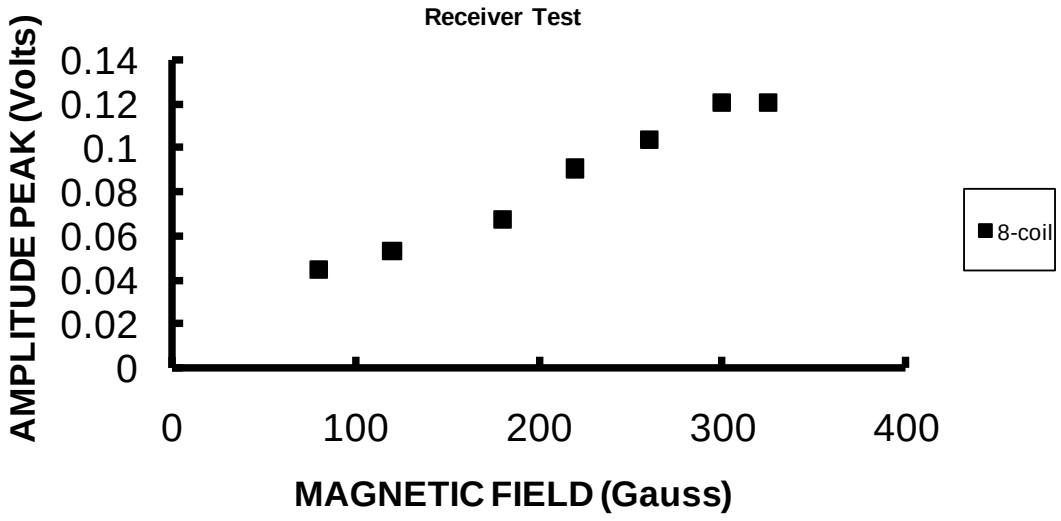

a)

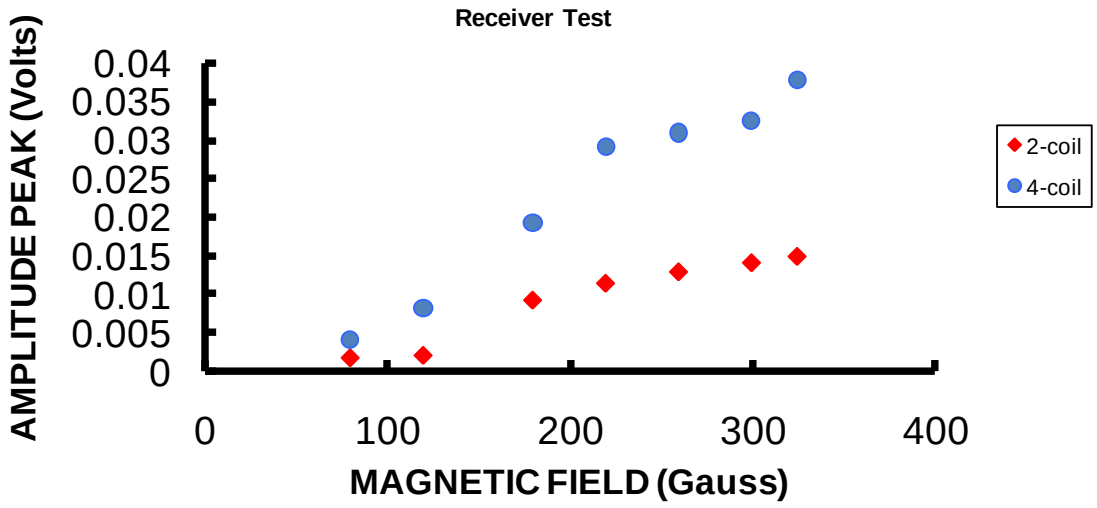

b)

Figure 28: Trend between the amplitude peak of the main signal detected and the applied magnetic field for a) 8-coil sensor b) 2-coil and 4-coil sensor.

In both the two cases (power and peak amplitude) there was increasing trend with an increase in the magnetic field for all the sensors.

4.1.2 Magnetic field tests results for the sensors of different number of coils placed as transmitters

Further tests were done to investigate the effect of increasing bias magnetic field on the amplitude of the signal generated when sensors of different number of coils (1-coil, 2-coil, 4-coil and 8-coil) were used as transmitters. The input voltage was 0.6 V and the receiver gain was 22 dB. A magnetic circuit setup was used for this testing. The magnetic field was varied from 80 G-325 G. Figure 29 shows the trend between the magnetic field applied to the transmitters (2-coil, 4-coil and 8-coil) and the power of the pulse detected by the receiver.

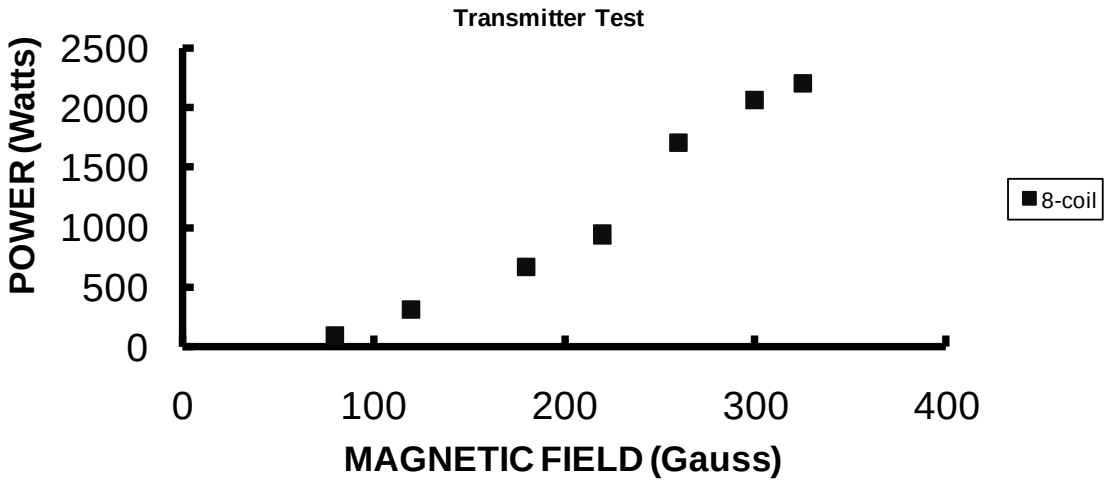

a)

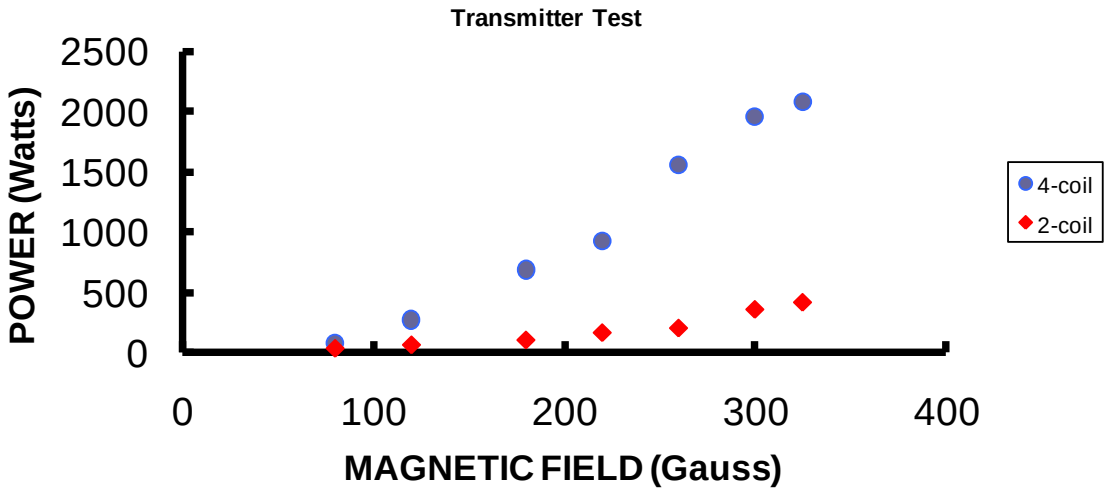

b)

Figure 29: Trend between the magnetic field and the power of the pulse detected by the receiver when acted by a) 8-coil transmitter and b) 4-coil transmitter and 2-coil transmitter.

The amplitude of the signal detected increased with the increase in the bias magnetic field levels of the transmitter.

4.2 Number of coils tests

4.2.1 Test results for sensors of different number of coils placed as receivers

The tests were done by placing 1-coil, 2-coil, 4-coil and 8coil sensors as receivers and the respective amplitudes of the signals detected have been recorded. The standard sensor was placed as a transmitter in all the cases. The number of coil turns was 50 per coil for all the sensors. A magnetic circuit set was used to apply the bias magnetic field. It was 240 G and constant in all the cases. The input voltage was 0.7 V and the receiver gain was 22 dB. Figure 30 shows the signal detected by the sensors of different number of coils at 240 G magnetic field.

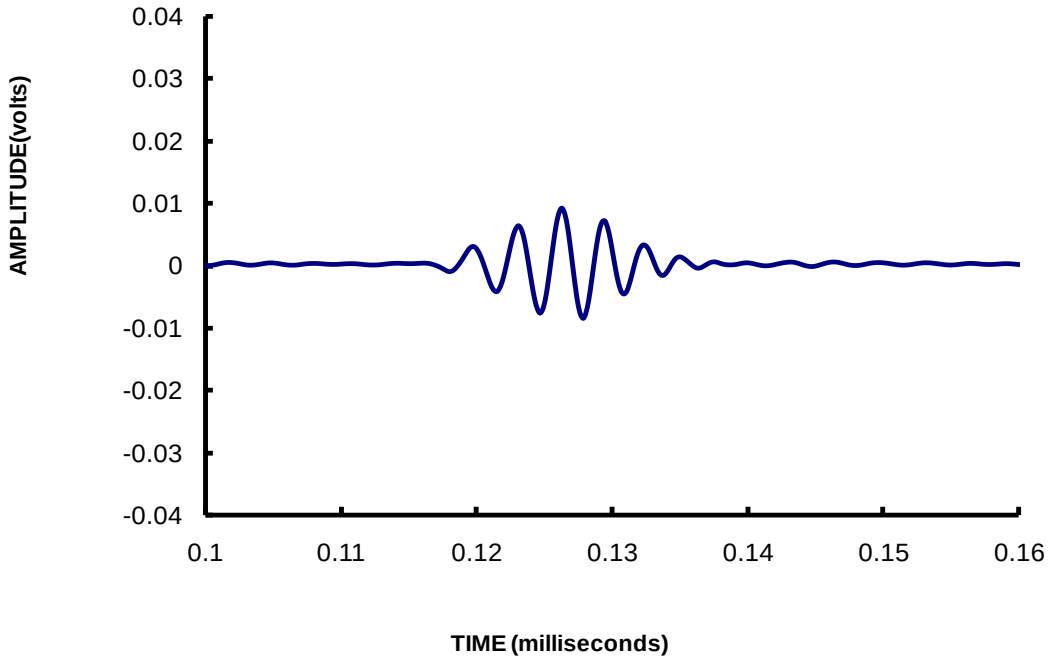
0.04
0.03
0.02
0.01
0
-0.01
-0.02
-0.03
-0.04
AMPLITUDE(volts)
0.1
0.11
0.12
0.13
0.14
0.15
0.16
TIME (milliseconds)

a)

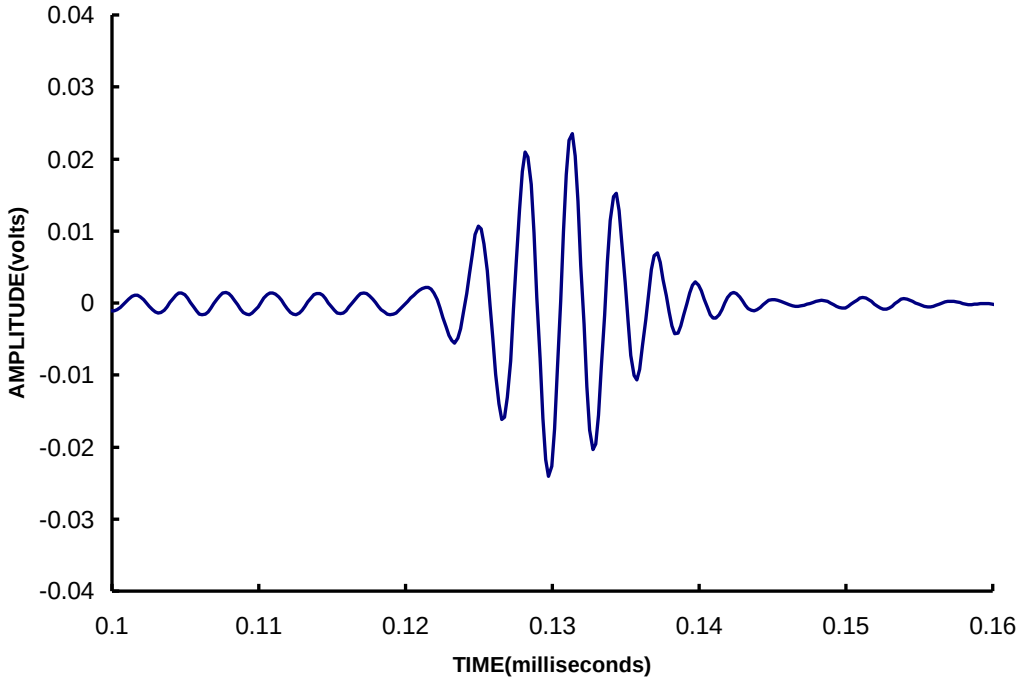
0.04
0.03
0.02
0.01
0
-0.01
-0.02
-0.03
-0.04
AMPLITUDE(volts)
0.1
0.11
0.12
0.13
0.14
0.15
0.16
TIME(milliseconds)

b)

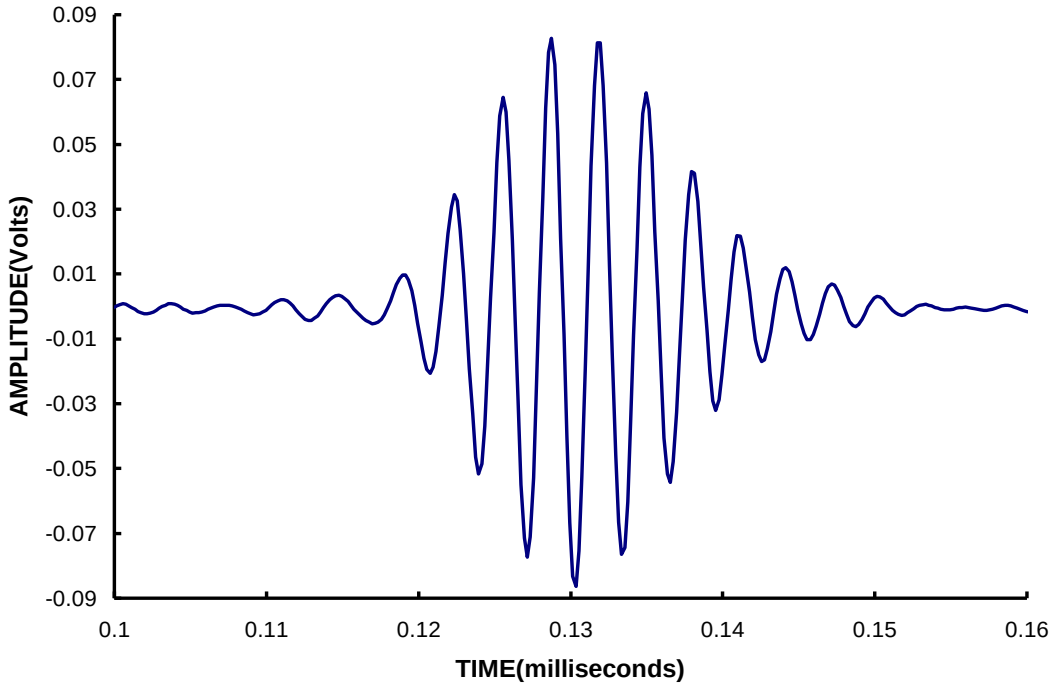

c)

Figure 30: Amplitude of the signal detected by a) 2-coil sensor b) 4-coil sensor c) 8-coil sensor at a magnetic field of 240 Gauss.

The amplitude of the signal detected increased with an increase in number of coils when the applied magnetic field remained the same. The following Figures show the power of the pulse detected by the sensors of different number of coils.

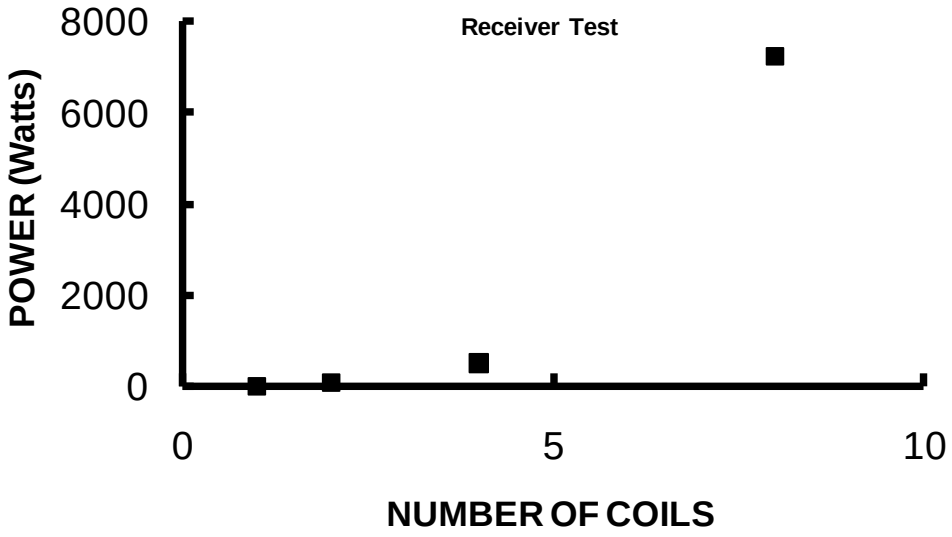

Figure 31: Graph showing the power of the signal detected by sensors of different number of coils.

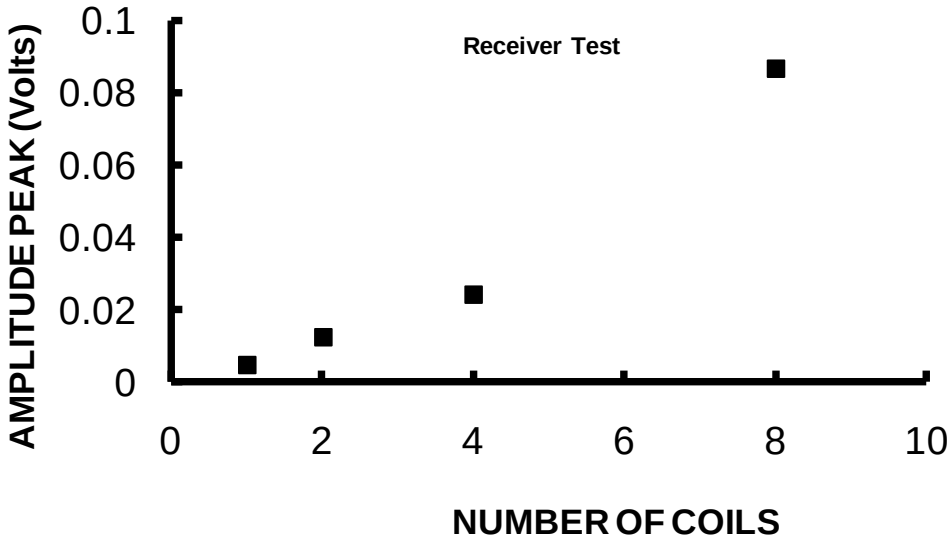

Figure 32: Graph showing the Peak amplitude of the signal detected by the sensors of different number of coils.

From Figure 31 and Figure 32 it could be observed in both the power and the peak amplitude of the signal detected by the sensors increased with an increase in the number coils when the magnetic field was 240 G in all the cases.

4.2.2 Test results for sensors of different number of coils placed as transmitters

The testing was done by placing 1-coil, 2-coil, 4-coil and 8coil sensors as pulsers and the respective amplitudes of the signals detected by the receiver have been recorded. The standard sensor was placed as a receiver in all the cases. For these tests the number of turns per coil was 50 and it remained constant. The magnetic circuit setup was used to apply the bias magnetic field. The bias magnetic field was 240 G in all the cases. The input voltage was 0.7 V and the receiver gain was 22 db.

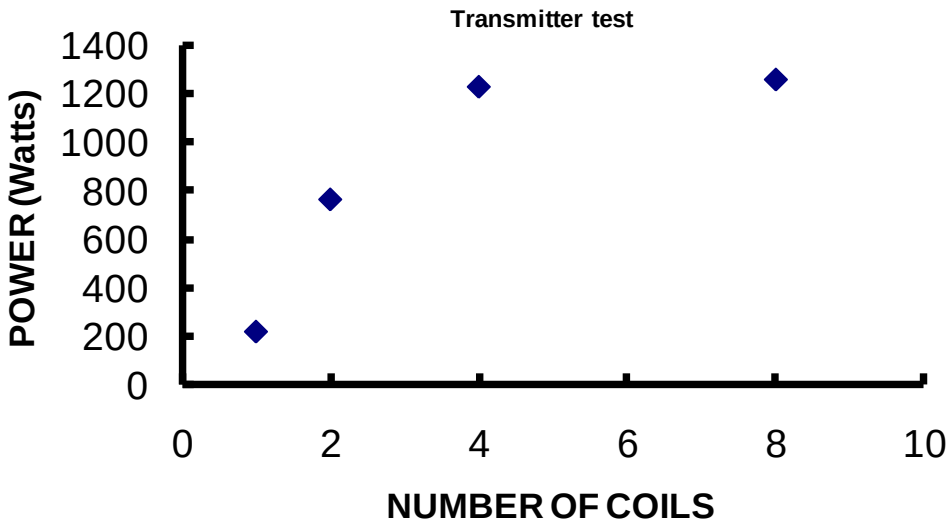

Figure 33: Trend between the power of the pulse detected by the receiver and the number of coils of the transmitter.

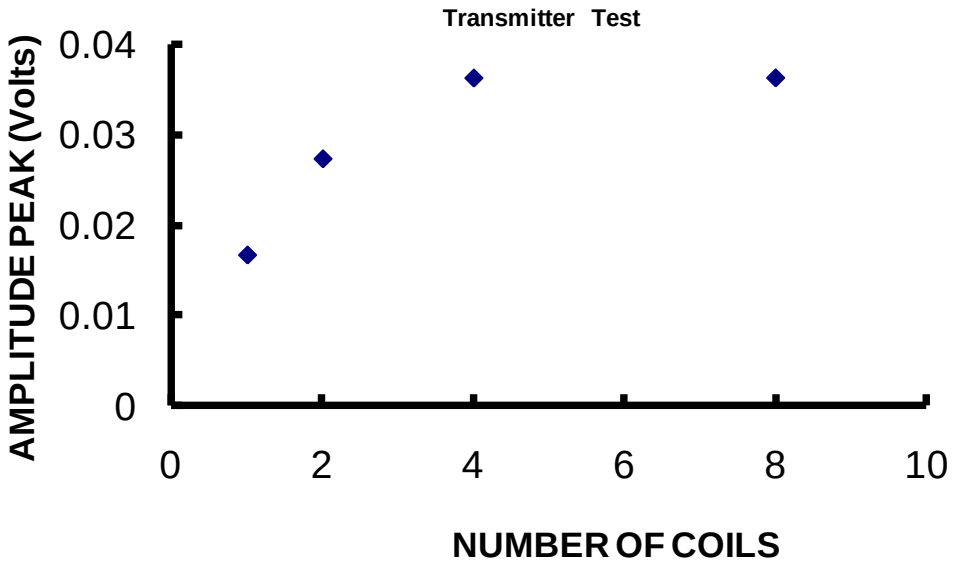

Figure 34: Trend between the Amplitude peak of the main signal detected by the receiver and the number of coils of the transmitter.

The amplitude of the signal detected by the receiver when an 8-coil sensor acted as a pulser is slightly greater than (almost equal to) that of the amplitude generated when a 4-coil transmitter is used which in turn is higher than the amplitude generated when acted by a 2-coil transmitter.

4.3 Number of windings tests

The sensors were tested for different number of coil turns while placed as receivers. A magnetic circuit setup was used to apply a constant bias magnetic field of 240 G. The input voltage for all the sensors was 0.7 V and the receiver gain was 30 dB. The following table gives the details of the test.

Sensor	Number of windings for which the sensors were tested	Magnetic field
1-coil	50,100,150,250	240 G
2-coil	100 (50 per coil), 150 (75 per coil), 200 (100 per coil) and 300 (150 per coil)	240 G
4-coil	200 (50 per coil), 300 (75 per coil),400 (100 per coil) and 600 (150 per coil)	240 G
8-coil	320 (40 per coil), 400 (50 per coil) and 600 (75 per coil)	240 G

Table 3: Table showing the type of sensor, the magnetic field applied and the different number of coil turns for which each sensor was tested.

Figure 35 shows the maximum signal obtained by each sensor by varying the number of coil turns.

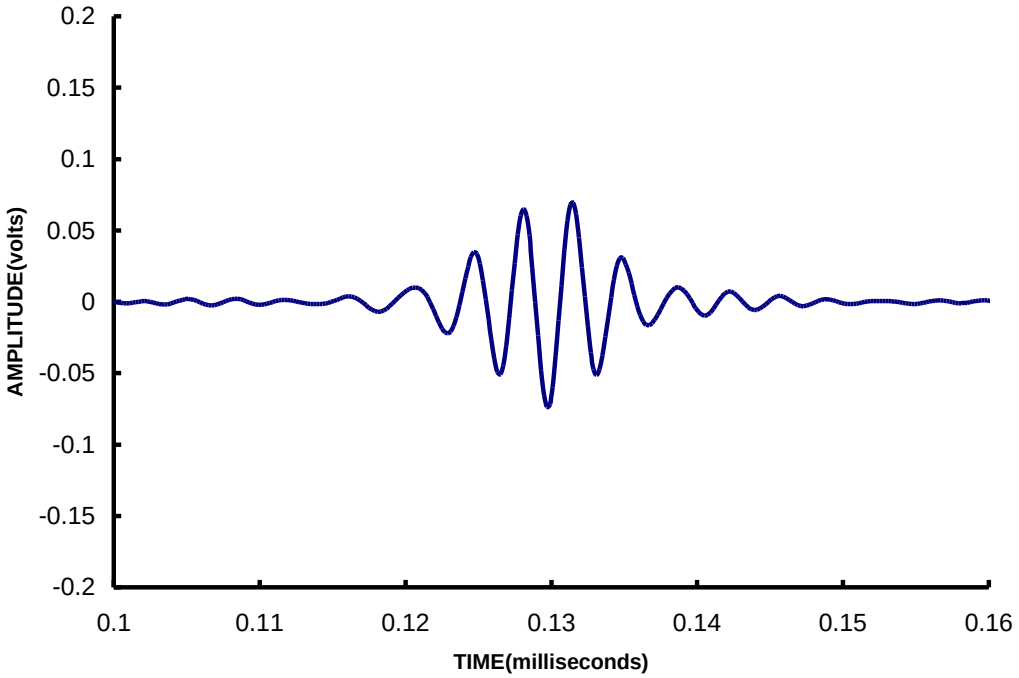
0.2
0.15
0.1
0.05
0
-0.05
-0.1
-0.15
-0.2
AMPLITUDE(volts)
0.1
0.11
0.12
0.13
0.14
0.15
0.16
TIME(milliseconds)

a)

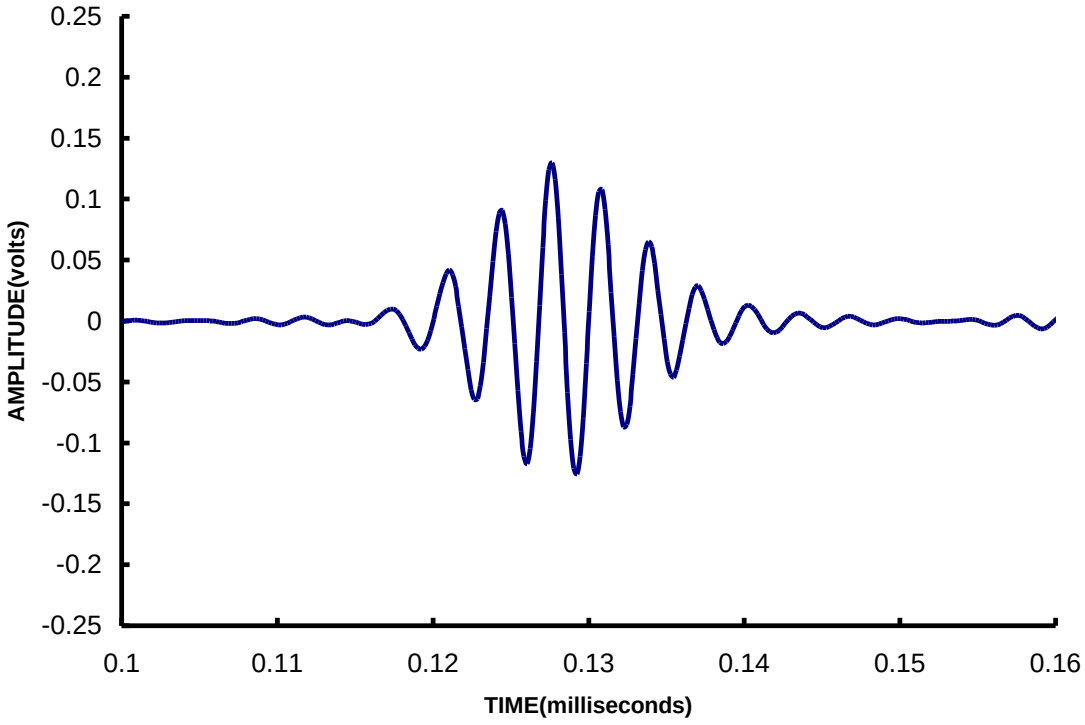
0.25
0.2
0.15
0.1
0.05
0
-0.05
-0.1
-0.15
-0.2
-0.25
AMPLITUDE(volts)
0.1
0.11
0.12
0.13
0.14
0.15
0.16
TIME(milliseconds)

b)

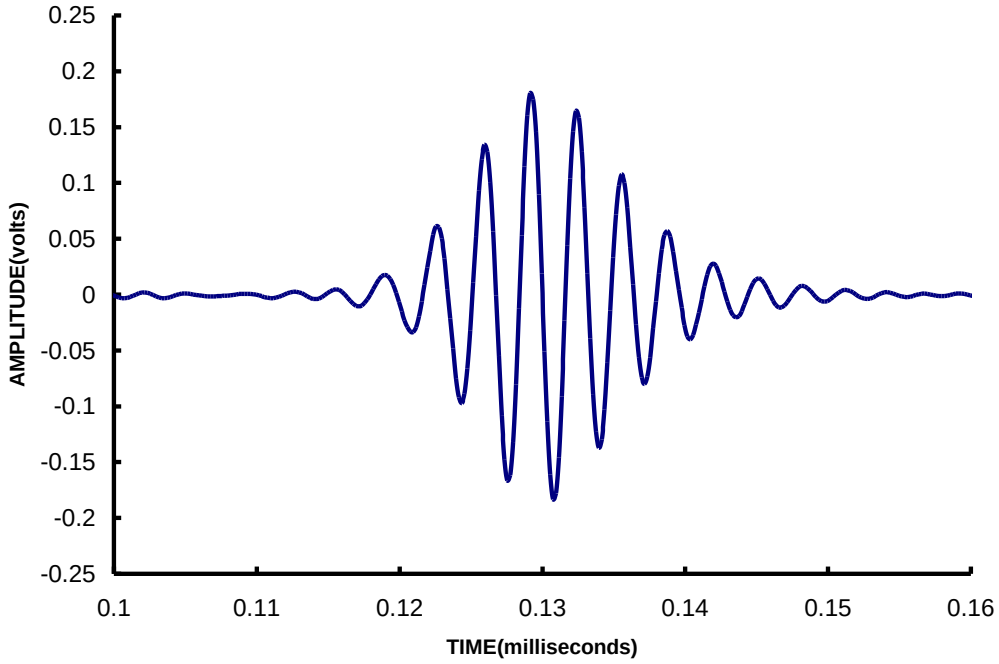

c)

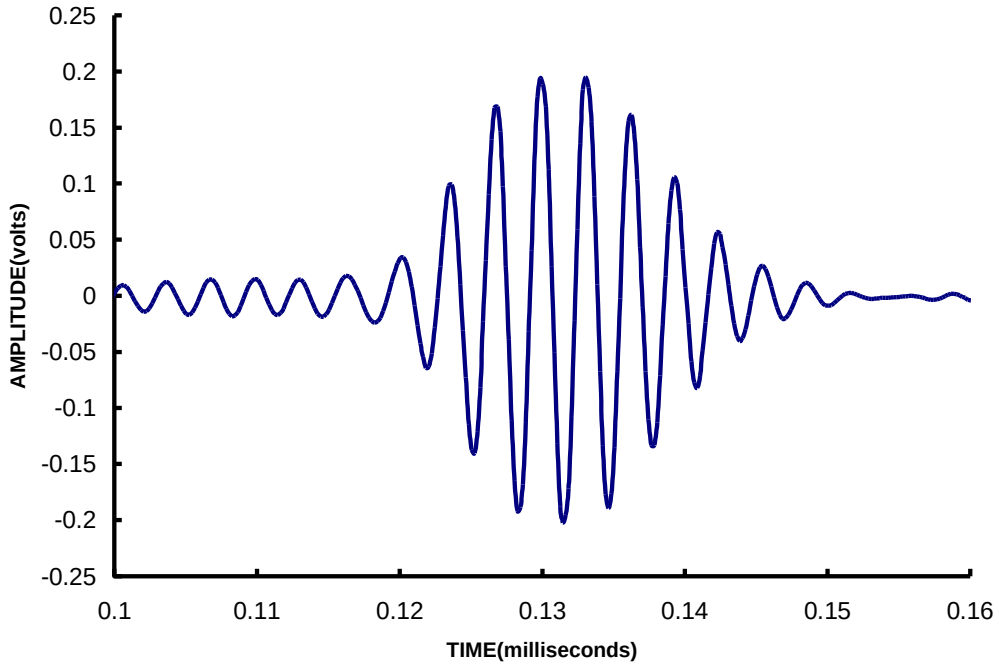

d)

Figure 35: Amplitude of the main signal detected by a) 1-coil sensor for 150 turns per coil, b) 2-coil sensor for 100 turns per coil, c) 4-coil sensor for 75 turns per coil d) 8-coil sensor for 50 turns per coil.

For an 8coil sensor highest amplitude was recorded when the number of windings was 50 per coil (50*8=400-turns), for a 4coil sensor it was recorded when the number of windings was 75-per coil (75*4= 300-turns), for a 2-coil it was 100 per coil (100 *2 = 200 turns) and for a 1-coil it was 150-turns.When the number of coil turns was increased beyond the above mentioned values the amplitude of the signal decreased

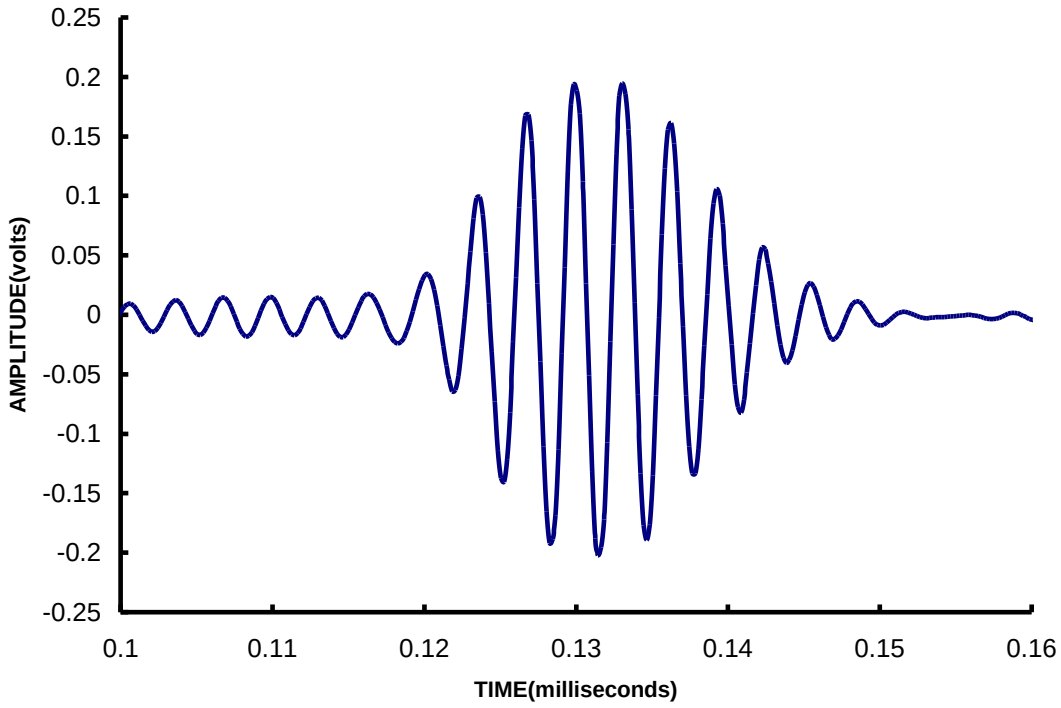

a)

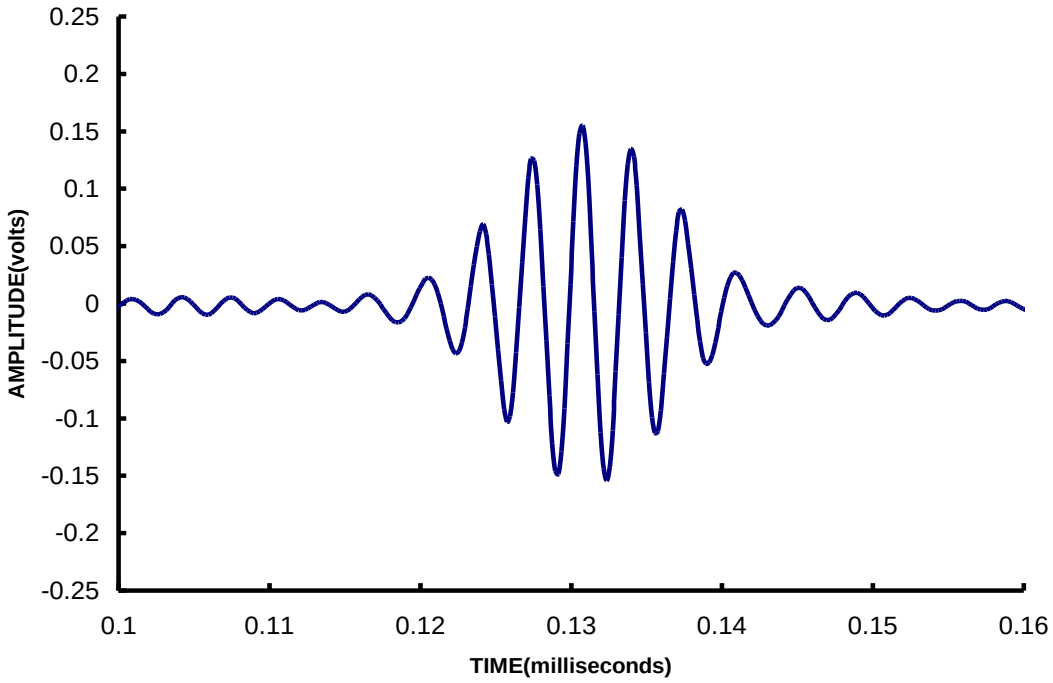

b)

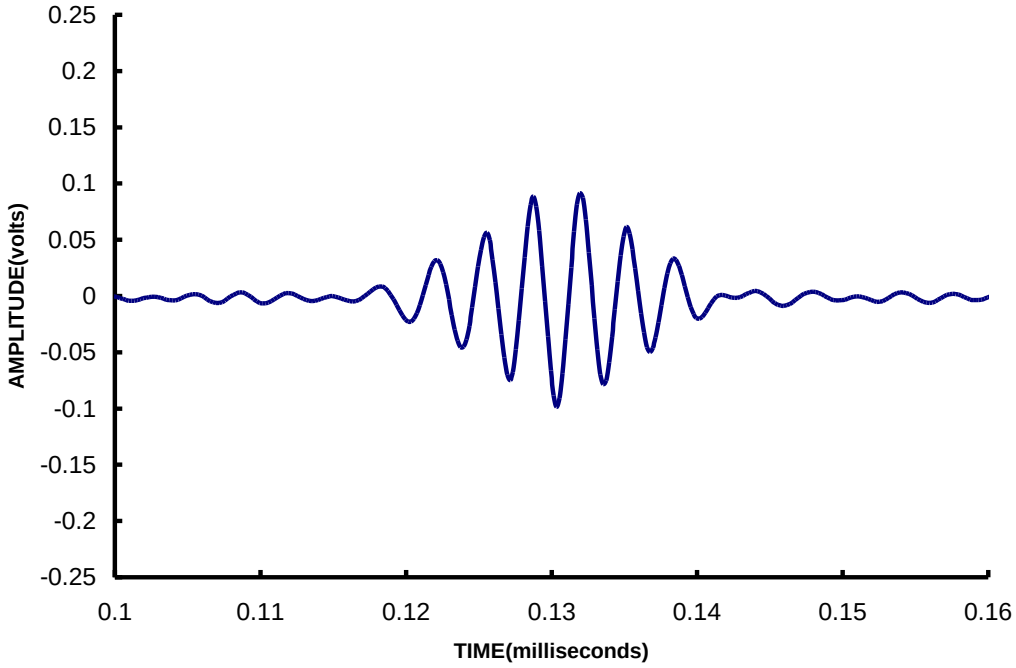

c)

Figure 36: Amplitude of the main signal detected by an 8-coil sensor for a) 400 turns (50 turns per coil), b) 500 turns (62 turns per coil), and c) 600 turns (75 turns per coil).

From the above shown graphs it could be noticed that the amplitude of the signal decreased as the number of coil turns increased beyond 50 per coil for an 8-coil.

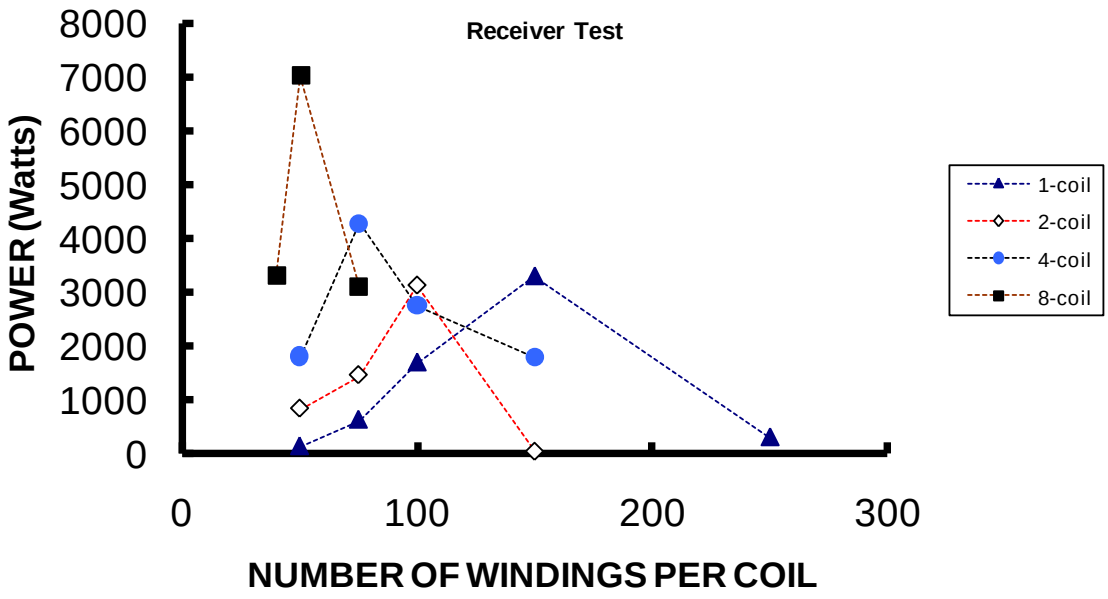

Figure 37: Graph showing the power of the pulse detected by the receivers for different number of coil turns.

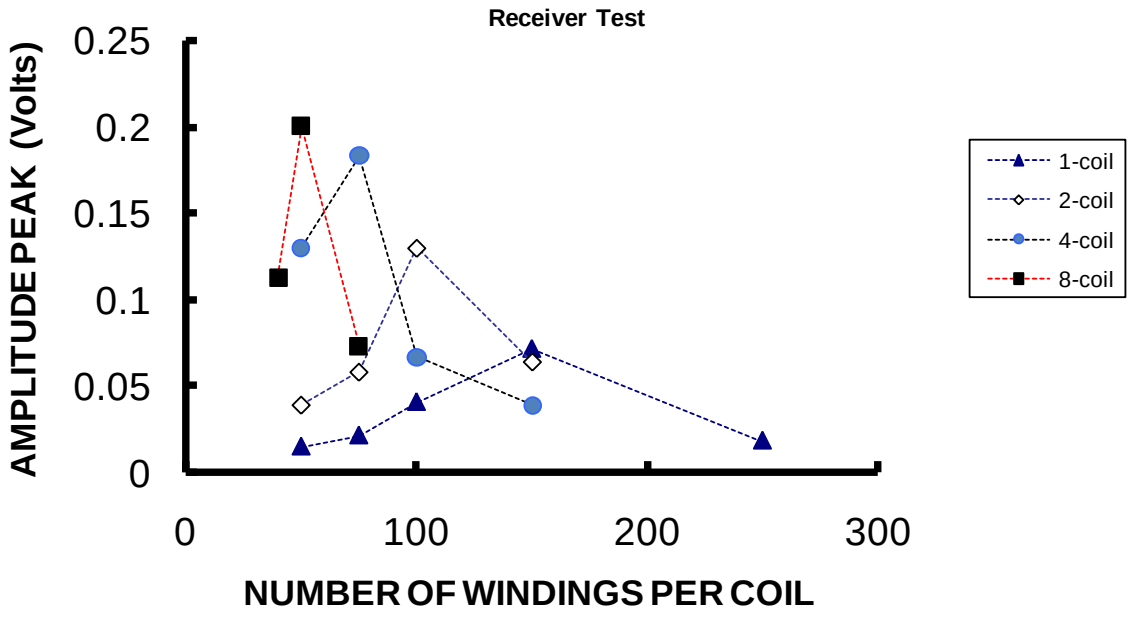

Figure 38: Graph showing the amplitude peak of the signal detected by the receivers for different number of coil turns.

The Amplitude of the pulse did not vary linearly with increase in the number of coil turns. With the magnetic field being the same for all the sensors, the amplitude generated by an 8-coil sensor with 50 windings per coil was greater than the other sensors. However it could be observed that the amplitude of the signal generated by an 8-coil sensor for 75 turns per coil is smaller when compared to a 4-coil sensor with 75 turns per coil. Similarly the signal generated by the 2-coil sensor for 100 turns per coil is larger than the signal generated by the 4-coil sensor for 100 turns per coil.

This is because though the number of windings per coil is the same for these sensors, the total number of windings changed with a change in number of coils i.e. in the first case for an 8-coil sensor 75 turns per coil would make a total of 600 windings (75*8) and for a 4-coil sensor it would be 300 windings (75*4) and similarly in the second case the total

number of windings for both the sensors (2-coil and 4-coil) was different. As a result, probably due to impedance factor the efficiency of a sensor with very high number of windings i.e. an 8-coil sensor with 600 windings is less than that of a 4-coil sensor with 75 windings per coil (300 turns).

4.4 Discussion

The variation in design parameters such as bias magnetic field, number of windings per each coil (number of coil turns) and number of coils had a considerable effect on the amplitude of the signal detected by the sensor. The effect of each design parameter on the efficiency of the sensor is discussed below.

Bias Magnetic field

Two different magnetic setups were used for the magnetic field tests performed and the trend of the signal produced was different with the two setups. In the first setup for cylindrical magnets the signal produced by the receiver initially decreased till certain point and then started increasing with an increase in the bias magnetic field.

In the second setup where a magnetic circuit setup was used, the amplitude of the signal generated increased with an increase in the bias magnetic field. Though from the results (Figure 39) peak amplitude region of the signal detected by the magnetic circuit setup and the cylindrical magnets setup look almost the same, it should be noted that in the set up for cylindrical magnets an input voltage of 0.8 V and 30 dB receiver gain was used while in the magnetic circuit setup much lesser input parameters such as 0.6 V input voltage and 22 dB receiver gain were used. Hence it could be understood that the efficiency of the sensor obtained using the magnetic circuit setup was much greater than that of the setup for cylindrical magnets.

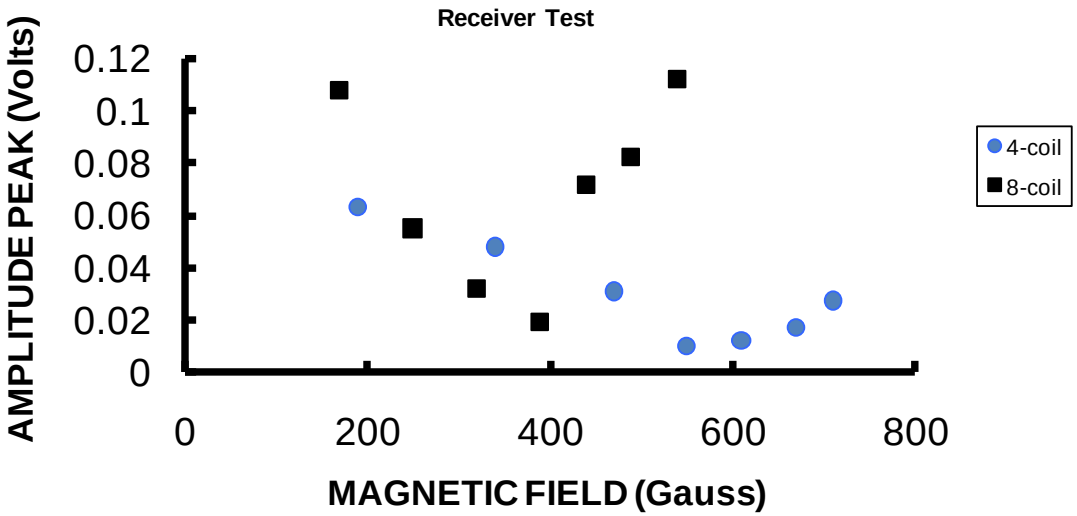

a)

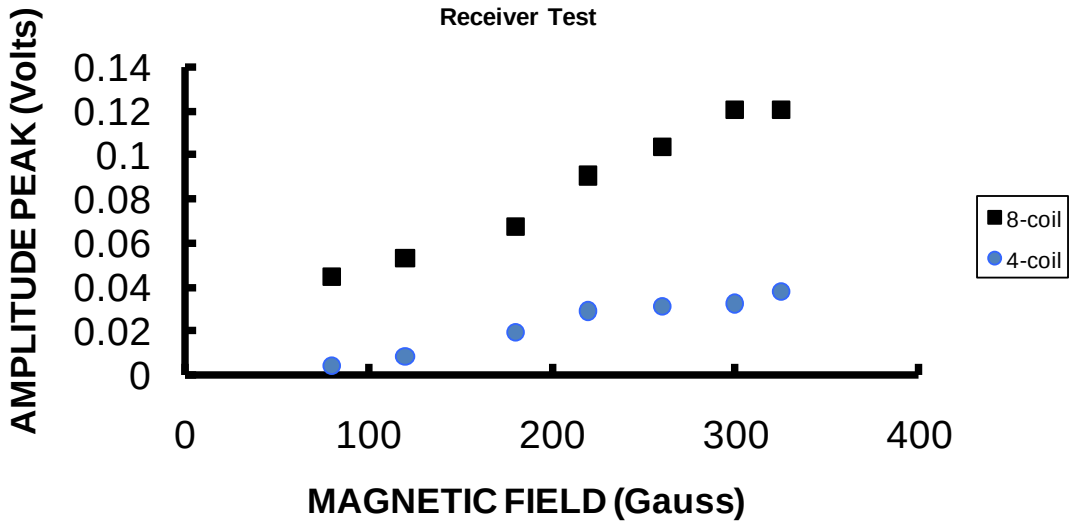

b)

Figure 39: Trend between the amplitude peak detected by the sensors and the magnetic field for a) Setup for cylindrical magnets and b) Magnetic circuit setup.

The theory behind the magnetostriction and the amplitude of the wave signal is discussed as follows. As discussed earlier magnetostriction process is the resulting strain in a material in the presence of magnetic field. Magnetostriction takes place due to magnetic domain reorientation. A magnetic domain is the region in the material with uniform magnetization i.e all the atoms within a magnetic domain are grouped together and aligned with one another. In an unmagnetized object though the atoms with in a magnetic domain are aligned in the same direction, but the alignment of the atoms changes from domain to domain i.e. different domains point in different directions. When the object becomes magnetized, the all the magnetic domains reorient themselves in the direction of the magnetic field. This magnetic domain reorientation causes a strain in the material. Magnetic reorientation occurs due to two processes; Domains realignment, where the domains that are favorably inclined with respect to the magnetic field grow at the expense of those that are aligned in opposite directions to the field and Rotation magnetization or domain rotation, where the favorably aligned domains rotate into the direction of the magnetic field. Domain realignment occurs at low magnetic fields while the domain rotation takes place at moderate and moderately high magnetic fields. At very high magnetic fields saturation of magnetostriction occurs.

Previous studies propose that when the domain realignment is dominant the magnetostriction of steel increases(region XY in Figure 40) and once the domains are aligned (region YZ in Figure 40) and rotation magnetization starts, the magnetostriction of steel starts decreasing [30] .

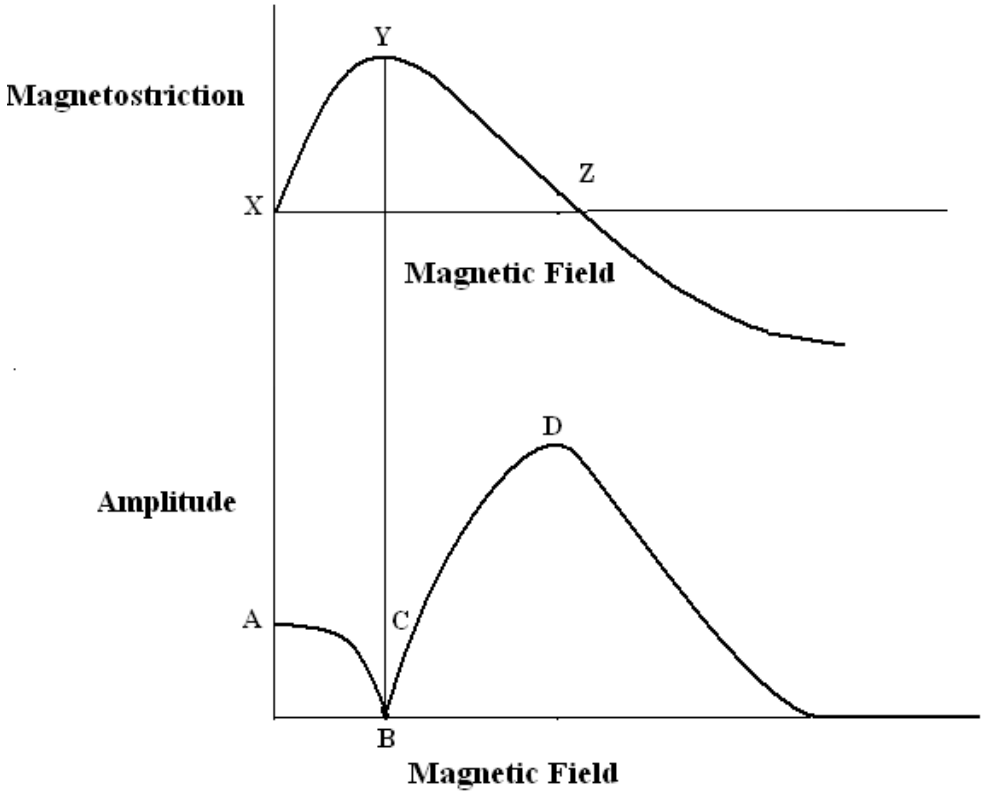

Figure 40: Magnetostriction curve for steel (upper) and the efficiency of an EMAT (below) as a function of magnetic field [31].

A relationship was obtained between the magnetostriction of steel and the excited longitudinal wave amplitude of an EMAT by Masahiko and Hirotsugu[31]. It is shown in Figure 40. As the magnetostriction of steel increases, the amplitude of the signal decreases. At the maximum magnetostriction no wave is launched and when the magnetostriction starts decreasing, the amplitude of the signal starts increasing. Almost a similar trend was shown in Thompson model, which determines the relationship between the bias magnetic field and the amplitude of the signal produced by a lamb wave EMAT[32].

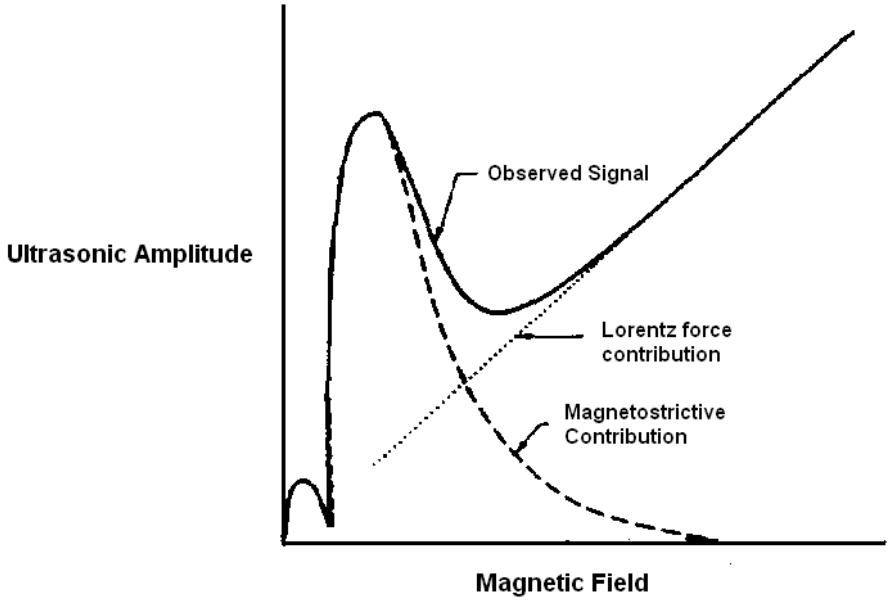

Figure 40: Graph showing the efficiency of an EMAT as a function of magnetic field [32].

Considering the above theories we could relate the trend obtained in our magnetic field tests using the cylindrical magnets setup to be in the region of ABC in Figure 40. The initial decreasing trend could be attributed to the fact that as the magnetic field was increased, the magnetostriction of steel started increasing due to domain realignment. As the magnetostriction increased to reach the maximum, the amplitude of the signal gradually decreased to minimum. Once the domain realignment is complete and as the rotation magnetization starts, the magnetostriction of the strand starts decreasing as a result the amplitude of the signal started increasing.

The results from the magnetic circuit setup showed that the amplitude of the signal increased with an increase in the magnetic field. The initial decreasing trend observed with the setup for cylindrical magnets is not obtained here. One probable reason for not finding the initial decreasing trend might be because by using the magnetic circuit setup the applied bias magnetic field is high enough to realign the domains completely

and as a result the magnetostriction has already reached the maximum. Further increase in the magnetic field resulted in the decrease in the magnetostriction due to rotation magnetization. As a result the amplitude of the signal increased. The trend obtained from the magnetic circuit setup could be related to the region of BC in the Figure 40. From the results obtained it could be observed that the magnitude of the signal obtained in the magnetic circuit setup is greater than that of the cylindrical magnets setup. This result further strengthens the assumption that the trend obtained using the magnetic circuit setup lies in the region BC. However an exact conclusion could not be made as there was no common method of measuring the magnetic field.

Number of windings

Change in the number of windings changed the amplitude of the signal generated. However there was no linear relationship between the number of windings and the amplitude of the signal produced. At a constant bias magnetic field by increasing the number of windings per coil the efficiency of the signal could be increased. The number of windings at which optimum signal is produced is not the same for all the sensors and it differs with change in number of coils and also may be with dimensions of the sensor. In our case the maximum amplitude of the signal for a 8-coil sensor was found for 400 turns (50 windings per coil), for a 4-coil sensor it was for 300 turns (75 windings per coil), for a 2-coil it was for 200turns (100 turns per coil) and for a 1-coil it was for 150turns when used as receivers. And it could be observed that at 75 windings per coil the efficiency of a 4-coil sensor is greater than that of an 8-coil sensor.

Number of Coils

Increase in the number of coils had a huge impact on the sensor efficiency. For a constant magnetic field and total number of coil windings the amplitude of the signal produced greatly increased with the increase in the number of coils of the sensor.

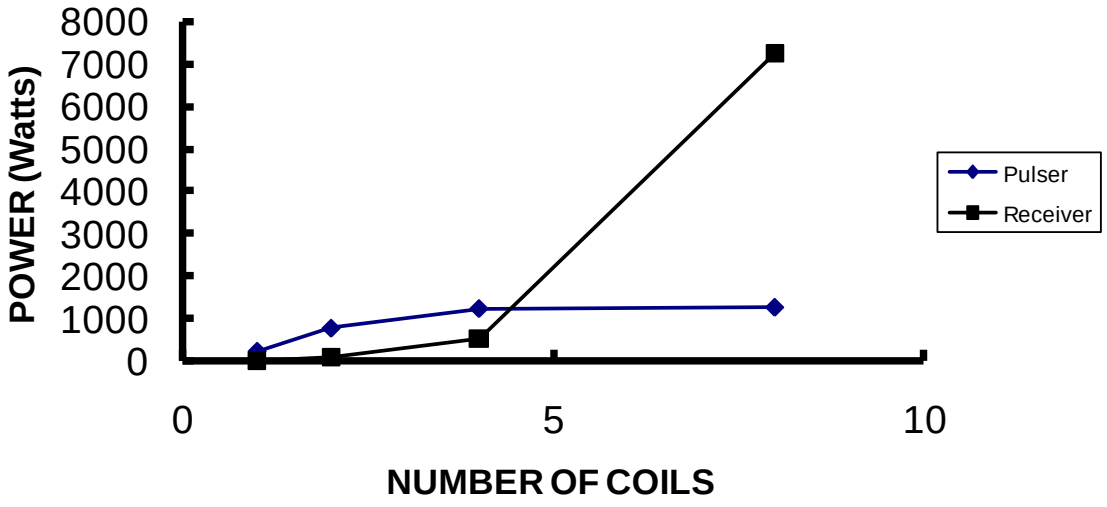

Figure 41: Trend between the power of the signal produced and the number of coils.

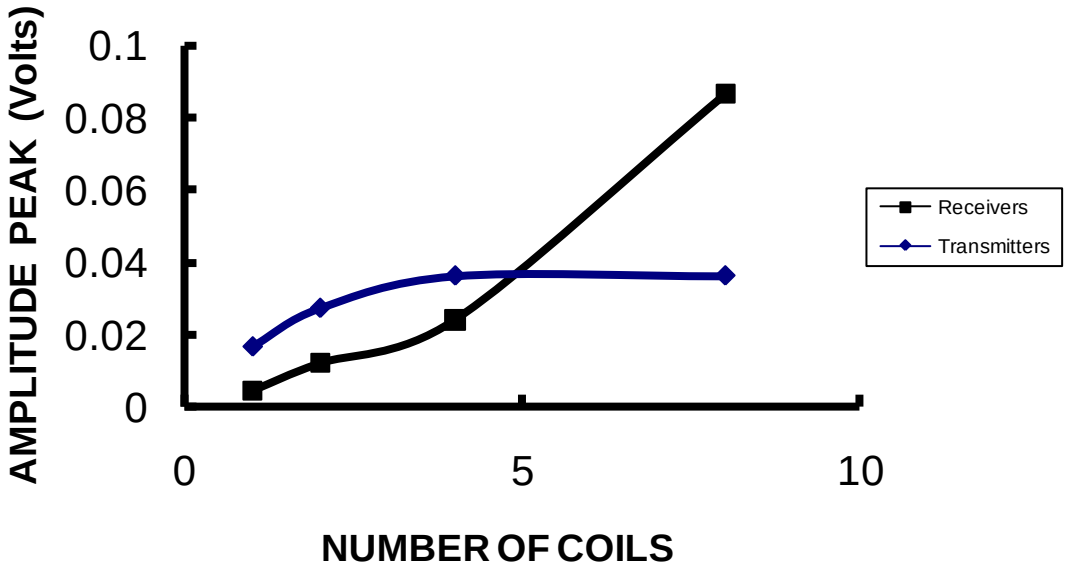

Figure 42: Trend between the peak amplitude of the signal produced and the number of coils.

From the graphs shown in Figure 41 and 42, a comparison could be drawn between the amplitude of the signal generated when 1-coil, 2-coil, 4-coil and an 8-coil sensor acted as receivers and transmitters. When the sensors acted as transmitters, the pulse detected by the standard sensor when an 8-coil pulser is used is almost equal to that of a 4-coil pulser which is much greater than the other pulsers (1-coil and 2-coil). That is not the case when these sensors were used as receivers. The difference in the power and amplitude of the pulse detected by an 8-coil receiver is much higher than the other sensors. In the first case when the number of coils in the receiver was increased the efficiency of the sensor increased while in the second case when the number of coils in the transmitter was increased the efficiency increased upto 4-coils, but was almost constant when 8-coil sensors were used.

5 CONCLUSIONS/FUTURE WORK

The following conclusions could be drawn based on the study done

- EMATs working on Magnetostrictive Phenomenon (*Joule* effect) have been successfully designed to launch and receive longitudinal waves at a frequency of 0.32 MHz.
- The efficiency of the sensor obtained using the magnetic circuit setup was much greater than that of the setup for cylindrical magnets
- The efficiency of the sensor increased with increasing magnetic fields for both transmitter and receiver tests at moderate to moderately high fields
- Cylindrical magnets setup appeared to provide low bias magnetic fields at which the efficiency of the sensor decreased with an increase in the magnetic field
- At a constant bias magnetic field and 50 windings per coil the efficiency of the sensor increased with an increase in number of coils
- Efficiency of receiver is more sensitive to number of coils than transmitter
- By varying the number of windings the efficiency of the sensor increased. However, the efficiency of the sensor when acting as a receiver did not vary linearly with the number of windings probably due to impedance factor. Based on the tests performed each sensor had optimized number of windings at which the efficiency was maximum. The values were 150 windings for 1-coil, 200 windings

for 2-coil, 300 windings for 4-coil and 400 windings for 8-coil. These are the total number of windings distributed evenly to each coil within the sensor.

5.1 Recommended sensor design

The maximum amplitude of the signal was observed for an 8-coil sensor. By varying the applied magnetic field levels and the number of windings the efficiency of the signal produced by an 8-coil sensor was further increased.

Therefore the recommended sensor design would be an 8-coil sensor with 400 windings (50 windings per coil). It could be used as a transmitter as well as a receiver to launch acoustic waves when embedded in concrete. With the maximized efficiency of the sensor we could probably overcome the wave attenuation problems and if so it would be the prominent step in the process of developing effective inspection technology for deterioration of embedded prestressing strand in concrete structures.

5.2 Future work/Recommendations

- A common method of measuring the magnetic field in the prestressing steel for different bias magnetic field setups would help in deriving an accurate relationship between the applied bias magnetic field and the sensor efficiency. One probable way of doing this could be by using Finite element modeling to analyze the magnetic flux generated for different magnetic setups.
- Considering the fact that magnetostriction of steel is stress sensitive, experiments could be conducted in order to evaluate the performance of the sensor when a prestressing strand is subjected to tensile loading.
- Experiments are to be conducted with the optimized EMAT sensors with a rod embedded in materials of different elastic stiffness in order to evaluate the effects

of wave attenuation and provide quantitative data on sensor performance when the strands are embedded in concrete.

REFERENCES

[1] A. T. Ciolko and H. Tabatabai, "Nondestructive Methods for Condition Evaluation of Prestressing Steel Strands in Concrete Bridges," *Final Report, NCHRP Project 10-53, National Cooperative Highway Research Program, Transportation Research Board, National Research Council*, 1999.

[2] G. A. Washer and R. E. Green, "Ultrasonic stress measurements in prestressing tendons," presented at Quantitative Nondestructive Evaluation. AIP Conference Proceedings, 2002.

[3] U. Nürnberger, "Corrosion induced failure mechanisms of prestressing steel," *Materials and Corrosion*, vol. 53, pp. 591-601, 2002.

[4] L. R. Kevin, J. W. Terry, and F. W. Klaiber, "Review of Nondestructive Evaluation Techniques of Civil Infrastructure," *Journal of Performance of Constructed Facilities*, vol. 11, pp. 152-160, 1997.

[5] R. A. Walther, "Mechanical Wave methods for In-Service Steel Bridge assessment," presented at Introduction to Nondestructive Evaluation Technologies for Bridges, Transportation Research Board Pre-conference Workshop, 2004.

[6] ASTM C 597-02, "Standard Test Method for Pulse Velocity through Concrete."

[7] H. H. Saleh, "Guidelines for selection of X-Ray Radiography systems for Evaluation of Highway Structures," presented at Introduction to Nondestructive Evaluation Technologies for Bridges, Transportation Research Board Pre-conference Workshop, 2004.

[8] G. A. Washer, "Testimony of the American Society of Civil Engineers," in *House Committee on Transportation and Infrastructure on Highway Bridge Inspections*, 2007.

[9] Z. Jinying and S. P. John, "Imaging Concrete Structures Using Air-Coupled Impact-Echo," *Journal of Engineering Mechanics*, vol. 133, pp. 628-640, 2007.

[10] M. C. Forde, "Ground Penetrating Radar," *Introduction to Nondestructive Evaluation Technologies for Bridges,* Transportation Research Board Pre-conference Workshop, 2004.

[11] G. A. Washer, "The Acoustoelastic Effect in Prestressing Tendons ", vol. Ph.D. Dissertation: Johns Hopkins University, 2001(A).

[12] P. C. Ken, J. C. Nicholas, and W. Glenn, "Health monitoring of civil infrastructures," *Smart Materials and Structures*, pp. 483, 2003.

[13] A. David, "Repairs without Rivets," in *Scientific American magazine*, November 2007.

[14] H. Ogi, "Field dependence of coupling efficiency between electromagnetic field and ultrasonic bulk waves," *Journal of Applied Physics*, vol. 82, pp. 3940-3949, 1997.

[15] X. Jian, S. Dixon, and S. B. Palmer, "In-plane and out-of-plane particle velocity measurement using electromagnetic acoustical transducers," presented at Ultrasonics Symposium, 2005 IEEE, 2005.

[16] X. Jian, S. Dixon, and R. S. Edwards., "Ultrasonic generation and optimization for EMAT," *Rev. Prog. Quant. Nondestr. Eval*, pp. 1041–1046, 2005.

[17] X. Jian, S. Dixon, R. S. Edwards, and J. Reed, "Coupling mechanism of electromagnetic acoustical transducers for ultrasonic generation," *The Journal of the Acoustical Society of America*, vol. 119, pp. 2693-2701, 2006.

[18] H. Landes, M. Kaltenbacher, and R. Lerch, "Large scale computation of coupled electro-acoustic systems using ANSYS and CAPA," presented at presented at the NAFEMS-Seminar, Computational Acoustics, 1999.

[19] P. J. Latimer and H. L. Whaley, "Electromagnetic Transducers for Generation and Detection of Ultrasonic Waves," *Acousto-Ultrasonics*, 1988.

[20] J. Krautkramer and H. Krautkramer, *Ultrasonic Testing of Materials*, 4 ed. New York: Springer Verlag, 1990.

[21] R. B. Thompson, "A Model for the Electromagnetic Generation of Ultrasonic Guided Waves in Ferromagnetic Metal Polycrystals," *Sonics and Ultrasonics, IEEE Transactions on*, vol. 25, pp. 7-15, 1978.

[22] S. Dixon, C. Edwards, and S. B. Palmer, "A laser-EMAT system for ultrasonic weld inspection," *Ultrasonics*, vol. 37, pp. 273-281, 1999.

[23] G. A. Alers and D. T. MacLauchlan, "High Frequency, Angle Beam EMAT's for Weld Inspection," *Review of Progress in Quantitative NDE*, vol. 2A, pp. 271-281.

[24] K. Youngkyu, K. Ikkyu, and K. Yoon Young, "Damage Detection by the Mode-Selectable Magnetostrictive Transducer for Cylindrical Ferromagnetic Waveguides," 2004.

[25] R. Polen, P. Latimer, W. Latham, D. MacLauchlan, and R. Neuschaefer, "EMAT Inspection of Space Shuttle External Tank Welds," presented at JANNAF Nondestructive Evaluation Subcommittee Meeting Proceedings, 1994.

[26] B. W. Maxfield, A. Kuramoto, and J. K. Hulbert, "Evaluating EMAT Designs for Selected Applications," *Materials Evaluation*, vol. 45, pp. 1,166 and 1,183, 1987.

[27] N. S. Tzannes, "Joule and Wiedemann Effects-The Simultaneous Generation of Longitudinal and Torsional Stress Pulses in Magnetostrictive Materials," *Sonics and Ultrasonics, IEEE Transactions on*, vol. 13, pp. 33-40, 1966.

[28] A. S. Morris, "Handbook of Intelligent Sensors For Industrial Automation, N. Zuech (Editor), Addison-Wesley, Reading, MA, 1992," *International Journal of Adaptive Control and Signal Processing*, vol. 11, pp. 257, 1997.

[29] S. Haykin and B. V. Veen, *Signals and Systems*, 2nd Edition ed, 2005.

[30] T. Yamasaki and Y. Uno, "High-Order Lamb Waves for Flaw Detection in Steel Plates by Electromagnetic Acoustic Transducers," *Journal of Solid Mechanics and Materials Engineering*, vol. 1 (2007) , No. 3, pp. pp.355-363, 2007.

[31] M. Hirao and H. Ogi, *"EMATs for science and industry," Noncontacting Ultrasonic Measurements*: Kluwer Academic Publishers, 2003.

[32] R. B. Thompson, "Detection of Strain by Measurement of the Efficiency of the Magnetostrictive Generation of Ultrasonic Surface Waves," *Ultrasonics Symposium*, pp. 585- 589, 1976.